

# A Review of Modeling and Applications of Energy Storage Systems in Power Grids

*This article covers the modeling and application of various energy storage systems into smart grid.*

By FABIAN CALERO<sup>✉</sup>, Member IEEE, CLAUDIO A. CAÑIZARES<sup>✉</sup>, Fellow IEEE, KANKAR BHATTACHARYA<sup>✉</sup>, Fellow IEEE, CHIOMA ANIEROBI, Member IEEE, IVAN CALERO<sup>✉</sup>, Member IEEE, MATHEUS F. ZAMBRONI DE SOUZA<sup>✉</sup>, Student Member IEEE, MOSTAFA FARROKHABADI, Member IEEE, NOELA SOFIA GUZMAN<sup>✉</sup>, Student Member IEEE, WILLIAM MENDIETA<sup>✉</sup>, Student Member IEEE, DARIO PERALTA<sup>✉</sup>, Student Member IEEE, BHARATKUMAR V. SOLANKI, Member IEEE, NITIN PADMANABHAN<sup>✉</sup>, Member IEEE, AND WALTER VIOLANTE

**ABSTRACT** | As the penetration of variable renewable generation increases in power systems, issues, such as grid stiffness, larger frequency deviations, and grid stability, are becoming more relevant, particularly in view of 100% renewable energy networks, which is the future of smart grids. In this context, energy storage systems (ESSs) are proving to be indispensable for facilitating the integration of renewable energy sources

Manuscript received 29 November 2021; revised 10 February 2022; accepted 7 March 2022. Date of publication 25 March 2022; date of current version 13 July 2023. This work was supported by the NSERC Energy Storage Technology (NEST) Network, Canada. (Corresponding author: Claudio A. Cañizares.)

Fabian Calero, Claudio A. Cañizares, Kankar Bhattacharya, Ivan Calero, Matheus F. Zambroni de Souza, Noela Sofia Guzman, and Dario Peralta are with the Department of Electrical and Computer Engineering, University of Waterloo, Waterloo, ON N2L 3G1, Canada (e-mail: fcalero@uwaterloo.ca; ccanizar@uwaterloo.ca; kankar@uwaterloo.ca; icalero@uwaterloo.ca; m6ferreirazambroni@uwaterloo.ca; nguzman@uwaterloo.ca; d2peralta@uwaterloo.ca).

Chioma Anierobi is with CPCS Canada, Ottawa, ON, Canada (e-mail: chiomaanierobi@gmail.com).

Mostafa Farrokhabadi is with Bluwave-ai, Inc., Ottawa, ON K2K 2A9, Canada (e-mail: mostafa.farrokhabadi@bluwave-ai.com).

William Mendieta is with the School of Electrical and Electronic Engineering, University College Dublin, Dublin, D04 V1W8 Ireland (e-mail: william.mendieta@ucdconnect.ie).

Bharatkumar V. Solanki is with Siemens Canada, Oakville, ON L6H 0H6, Canada (e-mail: bharat.solanki@siemens.com).

Nitin Padmanabhan is with EPRI International, Palo Alto, CA 94304 USA (e-mail: npadmanabhan@epri.com).

Walter Violante is with Terna, 00156 Rome, Italy (e-mail: walter.violante@gmail.com).

Digital Object Identifier 10.1109/JPROC.2022.3158607

(RESs), are being widely deployed in both microgrids and bulk power systems, and thus will be the hallmark of the clean electrical grids of the future. Hence, this article reviews several energy storage technologies that are rapidly evolving to address the RES integration challenge, particularly compressed air energy storage (CAES), flywheels, batteries, and thermal ESSs, and their modeling and applications in power grids. An overview of these ESSs is provided, focusing on new models and applications in microgrids and distribution and transmission grids for grid operation, markets, stability, and control.

**KEYWORDS** | Active distribution networks (ADNs); battery energy storage; compressed air energy storage (CAES); electricity markets; flywheel energy storage; microgrids (MGs); power system operation; power system stability and control; thermal energy storage; transmission systems.

## NOMENCLATURE

AA	Affine arithmetic.
ACE	Area control error.
ADN	Active distribution network.
AGC	Automatic generation control.
ATR	Alternate technologies for regulation.
BESS	Battery energy storage system.
CAES	Compressed air energy storage.

CAISO	California ISO.	SFR	Secondary frequency regulation.
CHP	Combined heat and power.	SHE	Sensitive heat storage.
DA	Day ahead.	SMES	Superconducting magnetic energy storage.
DAE	Differential and algebraic equation.	SoC	State of charge.
DER	Distributed energy resource.	SR	Spinning reserve.
DoD	Depth of discharge.	TCL	Thermostatically controllable loads.
DR	Demand response.	TG	Traditional generator.
EA	Energy arbitrage.	TESS	Thermal energy storage system.
EMS	Energy management system.	VSC	Voltage source converter.
EMT	Electromagnetic transient.	WECC	Western Electricity Coordinating Council.
EnC	Energy cost.		
ESS	Energy storage system.		
EV	Electric vehicle.		
EWH	Electric water heater.		
FESS	Flywheel energy storage system.		
GA	Genetic algorithm.		
GAD	Global adjustment.		
GAC	Genetic algorithm cost.		
GHG	Greenhouse gas.		
GSHP	Ground source heat pump.		
GT	Gas turbine.		
HOEP	Hourly Ontario energy price.		
HP	High pressure.		
HVAC	Heat, ventilation, and air conditioner.		
IBG	Inverter-based generator.		
ICT	Information and communication technology.		
ID	Idling reserve.		
IGBT	Insulated-gate bipolar transistor.		
IGV	Inlet guide vane.		
IESO	Independent electricity system operator.		
ISO	Independent system operator.		
IM	Induction machine.		
IRR	Internal rate of return.		
KLFN	Kasabonika Lake First Nation.		
LMP	Locational marginal price.		
LP	Low pressure.		
MARR	Minimum acceptable rate of return.		
MCS	Monte Carlo Simulation.		
MG	Microgrid.		
NARX	Nonlinear autoregressive exogenous.		
NN	Neural network.		
NYSO	New York ISO.		
OD	Oscillation damping.		
PCC	Point of common coupling.		
PFC	Primary frequency control.		
PFR	Primary frequency regulation.		
PH	Pump hydro.		
PID	Proportional, integral, and derivative.		
PMSM	Permanent magnet synchronous machine.		
PSS	Power system stabilizer.		
PV	Photovoltaic.		
RES	Renewable energy sources.		
RO	Robust optimization.		
RT	Real time.		
RTO	Regional transmission organization.		
SC	Supercapacitor.		
SFC	Secondary frequency control.		

## I. INTRODUCTION

Generation resources have evolved during the last few decades to address the issues of environmental pollution and GHG emissions. This has led to the development and penetration of a wide mix of RESs as well as DERs, in particular, IBGs such as PV, wind, small natural-gas-fueled generators, as well as controllable loads, EVs, and ESSs. These are modifying the traditional power system structure to create smart grids that contain decentralized medium- and low-voltage networks based on DERs, namely, ADNs and MGs [1]–[3]. This new grid paradigm is shown in Fig. 1, where ICTs play a significant role, transforming power grids into cyber-physical systems.

The stochastic nature of RES, with their dependence on weather conditions that results in intermittent operation, requiring adequate generation-load balancing and reserve capacity, is some of the fundamental issues to be considered in the planning and operation of these new grids for stability and reliability [4], [5]. In traditional schemes, system solutions, such as load shifting through demand management controls and interconnection with external grids, have been used to address these problems [6]. However, as penetration of RES increases, the use of ESSs is one of the most promising approaches to counteract these problems and facilitate full integration of RES into the grids, as part of DER deployment [7]. In fact, ESS paired with both small- and large-scale RES facilities has become a common practice in recent years, as prices of storage continue to decrease [8]. This configuration has several advantages, including decoupled time dependence of RES and the system demand needs, which is particularly relevant for PV generation that is available at a specific time window during the day, thus increasing reliability. It may also turn RES facilities into dispatchable generators, thus helping grid operators to reduce the uncertainty in their resources forecasting. The economic performance of coupled RES and ESS facilities is subject to market conditions and access to incentives and tax credits [9]. Thus, ESSs are currently being developed and deployed in small-, medium-, and large-scale applications to improve the technical and economic performance of smart grids since they not only have the capability of exchanging power with the grid but also can provide grid services, such as voltage and frequency regulation, which can contribute to improved system stability [10], in particular in the case of MGs operating in island mode [11].

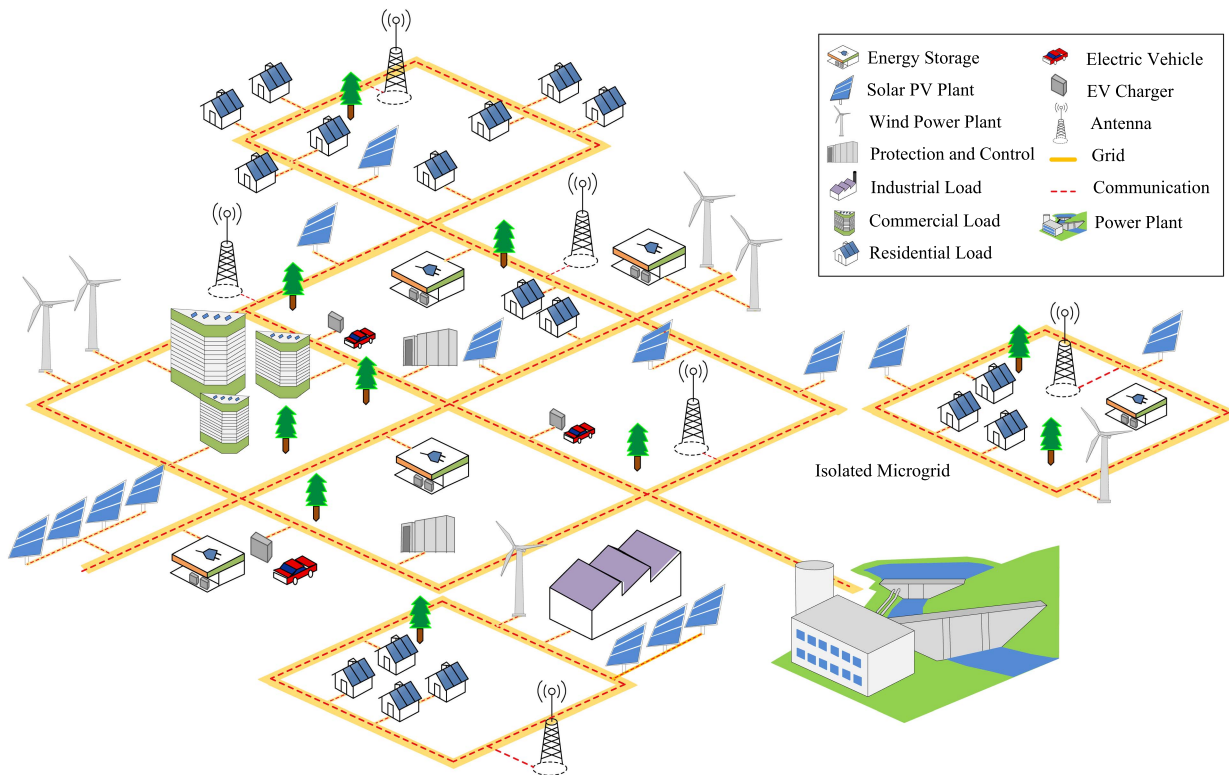


**Fig. 1.** Renewable-based smart grids of the future.

MGs have been and are being used extensively for electrification of remote communities, which operate mostly as stand-alone systems. Dropping prices of PV and wind systems has led to their increased deployments in MGs, which has increased the concerns about security of supply, power quality, and resilience. Integration of ESSs is a promising solution to these problems [12], [13]. Therefore, understanding ESSs and their impact on interactions with the grid is becoming essential for MG/grid operators and planners, requiring appropriate modeling and control approaches [14]. This article, therefore, focuses on providing a comprehensive review of novel and distinct ESS models, controls, and operation of specific ESS technologies for applications in MGs and distribution and transmission systems, rather than focusing on generic ESS models and controls for particular grid applications such as in, e.g., [14]. Thus, it provides a complete overview of the state-of-the-art ESS technologies being used and studied, with their models and controls depending on the application considered, which include CAES, BESS, FESS, and TESS for frequency regulation, grid stability, voltage regulation, and ancillary services in various types of grids and a market context. Thus, in Section II, the main features of relevant and evolving ESS technologies, in particular, BESS, FESS, CAESs, and TESSs, are first discussed. In Section III, the latest on ESS modeling of BESS, FESS, CAES, and TESS is presented, focusing on grid dynamic models and controls, as well as market integration models of ESS. Some of the main applications of these ESS

technologies for transmission systems, ADNs, and MGs are reviewed in Section IV. Finally, the main conclusions on the state-of-the-art of ESS modeling, control, and applications are presented in Section V, together with a discussion of possible future advancements in these areas.

## II. OVERVIEW OF ENERGY STORAGE TECHNOLOGIES

Storing energy from the power grid usually involves an energy conversion stage that transforms the electricity into another form of energy that can be efficiently stored. Most ESSs for power grid applications classify the technologies based on the type of energy stored [15]–[19] as follows.

- 1) *Mechanical*: PH, CAES, and FESS.
- 2) *Electrochemical*: BESS, including all battery technologies such as lead-acid, lithium-ion (most common), NaS, Ni-Cd, and flow batteries.
- 3) *Electrical*: SCs and SMES.
- 4) *Thermal*: TESS, including SHE and GSHP technologies.

In Table 1, the main characteristics of the most relevant ESS technologies are summarized. This present article focuses on the various ESS technologies, their modeling, control, and application, that are commercially available and are being widely developed, studied, and deployed in MGs, ADNs, and transmission grids, namely, BESS, FESS,

**Table 1** Characteristics of ESS Technologies [20]–[24]

Technology	Power Density [kW/m <sup>3</sup> ]	Energy Density [kWh/m <sup>3</sup> ]	Power Rating [MW]	Energy Capacity [MWh]	Capital Cost [\$/kW]	Lifetime [years]	Cycling Times [10 <sup>3</sup> cycles]	Round-trip Efficiency [%]	Response Time	Maturity
PH	0.01-0.12	0.5-0.133	100-5,000	500-8,000	500-2,000	30-60	10-30	70-85	mins	Mature
CAES	0.04-10	0.4-20	5-300	≤1,000	400-1,800	20-40	8-12	42-54	sec-min	Developed
FESS	40-20,000	0.25-424	0.01-0.25	0.025-5	100-350	15-20	20-100	90-95	msec	Commercial
SMES	300-4,000	0.2-13.8	0.1-10	0.015	200-300	20+	>100	95	msec	Commercial
SC	15-4,500	1-35	0.03-0.3	0.0005	100-300	10-12	10-1,000	85-98	msec	Developing
TESS	-	80-500	0.01-300	-	200-300	5-40	-	30-80	slow	Developing
Li-ion	56-800	94-500	0-0.1	0.004-10	1,200-4,000	5-15	0.2-2	85-90	msc	Commercial
Lead-acid	10-400	25-90	0-20	0.001-40	300-600	5-15	0.2-2	85-90	msc	Mature
NiCd	38-141	15-150	0-40	6.75	500-1,500	10-20	1.5-3	60-90	msec	Commercial
VRB	2.5-33.4	10-33	0.03-3	2	600-1,500	5-10	>16	85	msec	Commercial
ZnBr	3-8.5	5.2-70	0.05-2	4	700-2,500	5-10	2-3.5	75	msec	Demonstration

CAES, and TESS. Thus, the main characteristics of these ESS technologies are presented next.

### A. Battery Energy Storage Systems

BESSs convert electrical energy into chemical energy, which is stored in lead-acid, Ni-Cd, or lithium-ion battery cells, with the latter being the most utilized in BESS due to their technical performance and relatively low cost, which has dropped considerably in recent years [25]. The scheme of a typical BESS is shown in Fig. 2, in which the power conditioning system comprises a bidirectional buck-boost dc-to-dc converter that connects a battery pack to the dc side of a VSC. The battery pack contains cells organized in series and parallel to achieve the desired voltage and power rating, respectively. The dc-to-dc converter raises the battery pack voltage to a level appropriate to connect to the VSC's dc side and controls the battery pack charging/discharging. The self-commutating VSC based on IGBTs can be controlled to allow four-quadrant operation, i.e., active and reactive power exchanged in both directions with the grid, while the dc-to-dc converter can be controlled to regulate the voltage on the dc side of the VSC. A low-pass *RL* filter connects the terminals of the VSC and the PCC with the grid.

BESSs are characterized by very fast response and are capable of providing regulation services, such as frequency and voltage regulation, low-frequency OD, improving the

system transient stability, and other ancillary services. BESSs have large energy density (40–7000 kJ/kg), which facilitates their deployment in relatively small spaces compared to other ESS technologies such as PH, and have high efficiencies in the order of 75%–97%, depending on the battery chemistry [15]. However, the large number of operating cycles and deep discharging affects the performance of the battery cells and the overall lifetime of BESS, which are issues that must be taken into consideration when providing grid services. Flow-battery-based BESSs partially solve these problems by separating the battery's electrolytes in tanks, which are then combined to produce the chemical reaction in a flow reactor. This configuration facilitates replacing the electrolytes when their quality has been affected by either profound discharging or excessive cycling; however, their efficiency is reduced by the operation of the additional equipment involved, such as shunt currents in the electrolytes and pumps to move them.

### B. Flywheel Energy Storage System

A flywheel stores energy in the form of inertia of a heavy rotating disk that spins at very high speeds, typically more than 10 000 r/min. A chamber encapsulates the rotor that is suspended by magnetic bearings, allowing its rotation without any physical contact between the static and moving parts. The chamber is a vacuum space to reduce losses arising due to air friction. The flywheel's

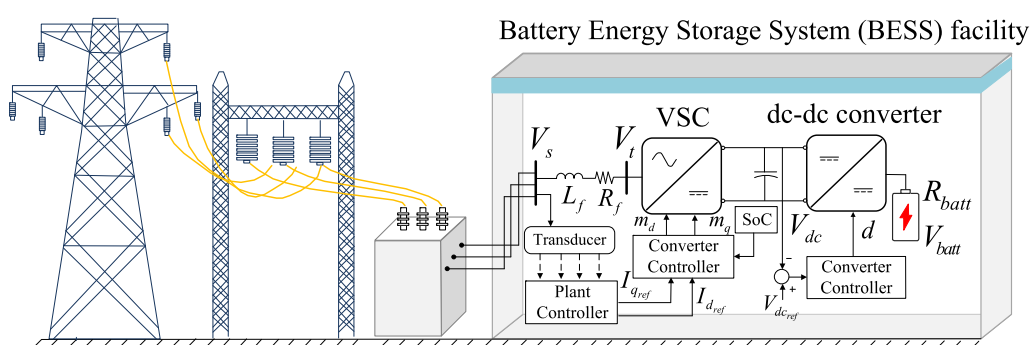


**Fig. 2.** Typical topology and control blocks of a BESS.

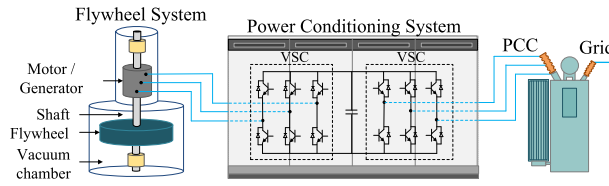


**Fig. 3. Flywheel components.**

rotor is connected to an electrical machine, which can be a PMSM or an IM; the former is preferred for applications requiring high rotational speeds, while the latter is better for high-power applications. The FESS power conditioning system can be based on dc-to-ac or ac-to-ac converters, or a combination of these; however, the most common topology comprises two back-to-back VSCs connecting the PCC and the machine, as shown in Fig. 3 [21], [26], [27]. The back-to-back configuration allows active power flow in both directions to charge and discharge the flywheel while also decoupling the flywheel's ac frequency from the grid's [26]. The energy storage capacity depends on both the speed and the combined inertia of the flywheel's rotor  $J_{FW}$  and machines rotor  $J_M$ , which is given by

$$E = \frac{1}{2}(J_{FW} + J_M)\omega_r^2 \quad (1)$$

where  $J_{FW}$  and  $J_M$  are constants; thus, the FESS charging/discharging energy can be controlled by regulating the rotor speed  $\omega_r$ .

FESSs have very fast response times (in millisecond) and high specific power (400–1500 W/kg) [15]; thus, along with BESS, they are ideal candidates to provide grid services such as frequency regulation. However, FESSs are superior in terms of cycling (>150 000 cycles) and DoD capability, which are two well-known issues that affect the BESS performance. Their round-trip efficiency is in the range of 75%–95% and has a typical life of 15–20 years [15]. Some existing flywheel facilities include the 2-MW Minto facility in ON, Canada [28], and the Beacon's 20-MW Stephentown and 20-MW Hazel facilities in NY and PA, USA, respectively [29].

### C. CAES System

In CAES, energy is stored as pressurized air in natural reservoirs such as an underground salt cavern or above-ground tank, with the latter being suitable only for small-scale applications. In the charging mode, a compressor physically coupled with a synchronous motor that draws power from the grid pressurizes the air, which is carried through pipes to the cavern. The heat produced in the compression process is removed by heat exchangers and can be stored for later use during expansion, thus improving the system efficiency. In the discharging mode, the air at HP is extracted from the cavern and expanded in a turbine that

is attached to the rotor of a synchronous generator that injects the power back to the grid.

In diabatic CAES, the air is preheated in a recuperator before the expansion using the remnant heat of the gases at the exhaust of the turbine and then combined with natural gas and burned in a combustion chamber to increase the temperature further [31], [32]. On the other hand, an adiabatic CAES does not burn gas and rather preheats the air using the compression heat stored. CAES can have a single synchronous machine interfacing with the grid, which operates as motor or as generator, or two independent machines; the latter allows simultaneous operation in charging and discharging modes and provides more flexibility in the design and size of the system. Through the synchronous generator, CAES can provide voltage and frequency regulation, but unlike other ESSs, they add inertia to the power grid. A typical CAES system is shown in Fig. 4.

Along with PH, CAESs are the only ESSs that are currently economically viable for bulk applications, with lifetimes longer than 40 years and efficiencies greater than equivalent GTs or combined cycle units, i.e., in the range of 30%–70%, depending on the type of CAES (diabatic or adiabatic) [33], [34]. They can provide black start, with start-up times of 10–12 min, and also have fast ramping capability, i.e., 25%/min. Currently, there are two large diabatic CAES projects operating worldwide, the 290-MW Huntorf facility in Germany [31] and the 110-MW McIntosh facility in AL, USA [32]. There are also small-scale pilot plants such as the adiabatic facility in Goderich, ON, Canada [35].

### D. Thermal Energy Storage Systems

They store heat in a reservoir that can be a tank [36], hot bricks [37], or an underground borehole [38], while the medium to transfer this heat can be liquid or gas. A generic TESS configuration is shown in Fig. 5. In the discharging mode (heating mode), the thermal load is supplied by the heat obtained from a thermal storage device through a heat exchanger, while in the charging mode (cooling mode), the heat is removed from the thermal load and transferred to the storage device through the heat exchanger. A pump is used to circulate the heat in both directions so that the TESS can be charged/discharged directly from/to the thermal load, whose heat depends on the application, such as supplying a building's heat needs during cold winter days or air conditioning (A/C) during summer days. Hence, an electrical interface is usually associated with the thermal load, allowing the TESS to discharge when the price of electricity is high or grid RES power is not available or to charge when the price is low or grid RES power is in excess.

TESSs have become popular for supplying the HVAC and water heating (WH) needs of households, especially in locations with cold weather, and the GSHP systems. In these systems, heat extracted from the house is pumped

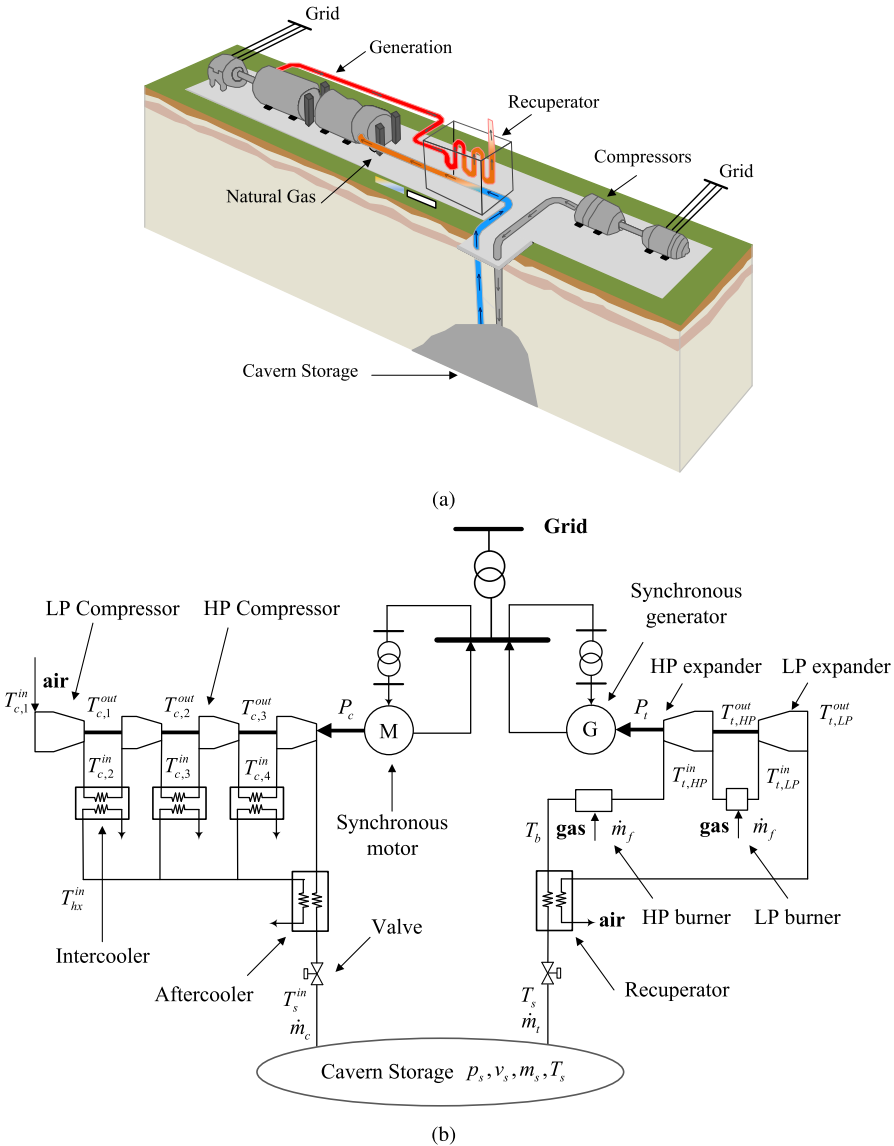


**Fig. 4.** Diabatic CAES: (a) physical system layout and (b) dynamic model for power system analysis [30].

to the ground and hence cool down the house during warm summer days, while the stored heat is pumped back to the house during winter, to provide space heating [38], [39]. Typically, one or multiple boreholes can be drilled into the ground in an external loop, which uses a pump to circulate the water mixed with antifreezing through a high-density polyethylene pipe, which acts as a heat exchanger between the fluid and the borehole surroundings, as shown in Fig. 6.

An evaporator transfers the heat from a refrigerant in an inner loop to the borehole loop. The refrigerant, whose circulation is through a compressor that further increases its temperature, carries the heat, extracted in a condenser, from the warm air moving through the ductwork in the house. A reversible valve in the inner loop allows charging the GSHP system by changing the direction of circulation of the refrigerant, thus also switching the tasks of the condenser and evaporator. By controlling the compressor, the heat transfer can be regulated, thus allowing the system to also provide short-term grid services such as frequency regulation [38] or participate in DR through aggregators [39]. Note that in this system, the electrical and thermal paths are physically decoupled.

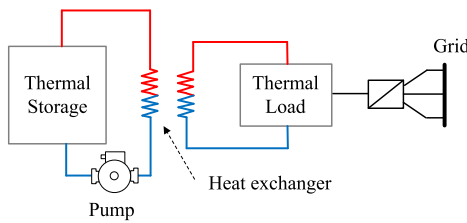


**Fig. 5.** Generic TESS.

### III. ESS MODELS

In this section, the state of the art on ESS modeling is discussed, focusing on the technologies described in

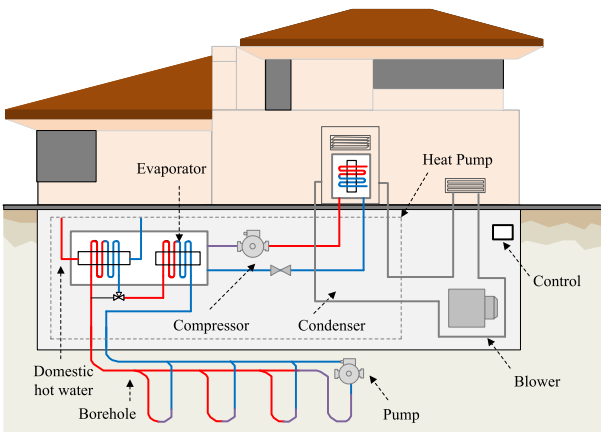


Fig. 6. GSHP system.

Section II and covering different modeling domains such as single models and aggregated dynamic models, and operation models at the wholesale electricity market level as well as at the ADN and MG level.

## A. Dynamic Models

1) *Battery Energy Storage System*: Depending on the application, the dynamic model of BESS can have different levels of complexity. For example, in EMT studies, MGs or unbalanced ADNs, a three-phase model of a VSC coupled with a dc-to-dc converter provides an accurate representation, as shown in Fig. 7. A further approximation may involve replacing the dc-to-dc converter with a constant voltage source and/or averaging the terminal voltage of the VSC, thus replacing the switches with controlled voltage sources. The former preserves the high-frequency response of VSC in the BESS, while the latter removes all high-frequency responses, resulting in a less-computationally demanding model [40].

For large power systems studies, averaged BESS models are more common, to be consistent with other system component models available, which often neglect high-frequency transients. In this context, the BESS can be modeled assuming balanced operation by a set of DAEs based on the system presented in Fig. 7 as follows [41]:

$$\dot{V}_{in} = -\frac{1}{C_2 R_{bat}} V_{in} - \frac{1}{C_2} I_L + \frac{1}{C_2 R_{bat}} V_{bat} \quad (2)$$

$$\dot{V}_{dc} = \frac{1-d}{C_1} I_L - \frac{1}{C_1} I_{dc} \quad (3)$$

$$\dot{I}_L = \frac{1}{L} V_{in} - \frac{1-d}{L} V_{dc} \quad (4)$$

$$I_{dc} = \left( \frac{3V_{sd}}{2M_c V_{dc}} \right) I_{sd} \quad (5)$$

$$V_{td} = \frac{1}{2} m_d V_{dc} \quad (6)$$

$$V_{tq} = \frac{1}{2} m_q V_{dc} \quad (7)$$

$$P_s = \frac{3}{2} I_d V_{sd} N_c \quad (8)$$

$$Q_s = -\frac{3}{2} I_q V_{sd} N_c \quad (9)$$

$$L_f \dot{I}_{sd} = V_{td} - V_{sd} - R_f I_{sd} + \omega_o L_f I_{qs} \quad (10)$$

$$L_f \dot{I}_{sq} = V_{tq} - V_{sq} - R_f I_{qs} - \omega_o L_f I_{ds} \quad (11)$$

where (2)–(4) model the dc-to-dc converter with  $V_{in}$ ,  $V_{dc}$ , and  $I_L$  representing the battery pack terminal voltage, dc-link voltage, and inductor  $L$  current, respectively; (5) is the link between the VSC and dc-to-dc converter, considering  $M_c$  dc-to-dc converters in parallel to achieve the VSC rated power; (6) and (7) are  $d$ - and  $q$ -axis components of the VSC's terminal voltage  $V_t$ , with modulation indices  $m_d$  and  $m_q$ ; (8) and (9) define the active  $P_s$  and reactive  $Q_s$  power injected by the BESS at the PCC, for a given voltage  $V_s$  and current  $I_s$ , comprising  $N_c$  VSCs in parallel to achieve the BESS rated power; and (10) and (11) denotes the ac filter equations in the  $d$ - and  $q$ -axes in terms of  $L_f$  and  $R_f$ . This model assumes that the battery pack is modeled as a fixed voltage source  $V_{bat}$  with a resistor in series  $R_{bat}$ , but a more complex model can be considered as well, which can include the SoC effect on  $V_{bat}$  as follows [40]:

$$V_{bat} = V_{bat_0} - K \frac{1}{SoC} + A^{-B(1-SoC)D} \quad (12)$$

where  $D$  is the battery capacity in Ah,  $K$  is the polarization voltage in V, and  $A$  and  $B$  are parameters that can be tuned to fit a specific battery model. Note that more complex representations of the battery pack may be used (e.g., [42]); however, these will increase the computational burden, especially when other grid components are also modeled. On the other hand, the voltage source in series with a resistor shown in Fig. 7 balances accuracy and complexity, to allow capturing relevant battery issues for most grid studies and applications, such as aging or degradation, which can be readily modeled through reduced values of  $V_{bat}$  and increased values of  $R_{bat}$  [43].

In actual BESS facilities, multiple VSC, multiple dc-to-dc converters per VSC, and battery cell arrays may be needed depending on the facility's size [44]. Modeling each of these components individually may be computationally cumbersome for grid studies; therefore, a common practice consists of representing only one VSC and one dc-to-dc converter per VSC when this converter is modeled, assuming a simple aggregation of active and reactive power injected into the grid, as shown in Fig. 7.

2) *Compressed Air Energy Storage*: The dynamics associated with the mechanical and thermal subsystems are relevant in frequency regulation and frequency stability studies, and thus, these need to be modeled. Conversely, transient stability or EMT studies are not focused on slow dynamics and hence are more important to model the electric machines (generator/motor) and their controls in some detail. However, it has been demonstrated that some fast-acting mechanical power controls may have a

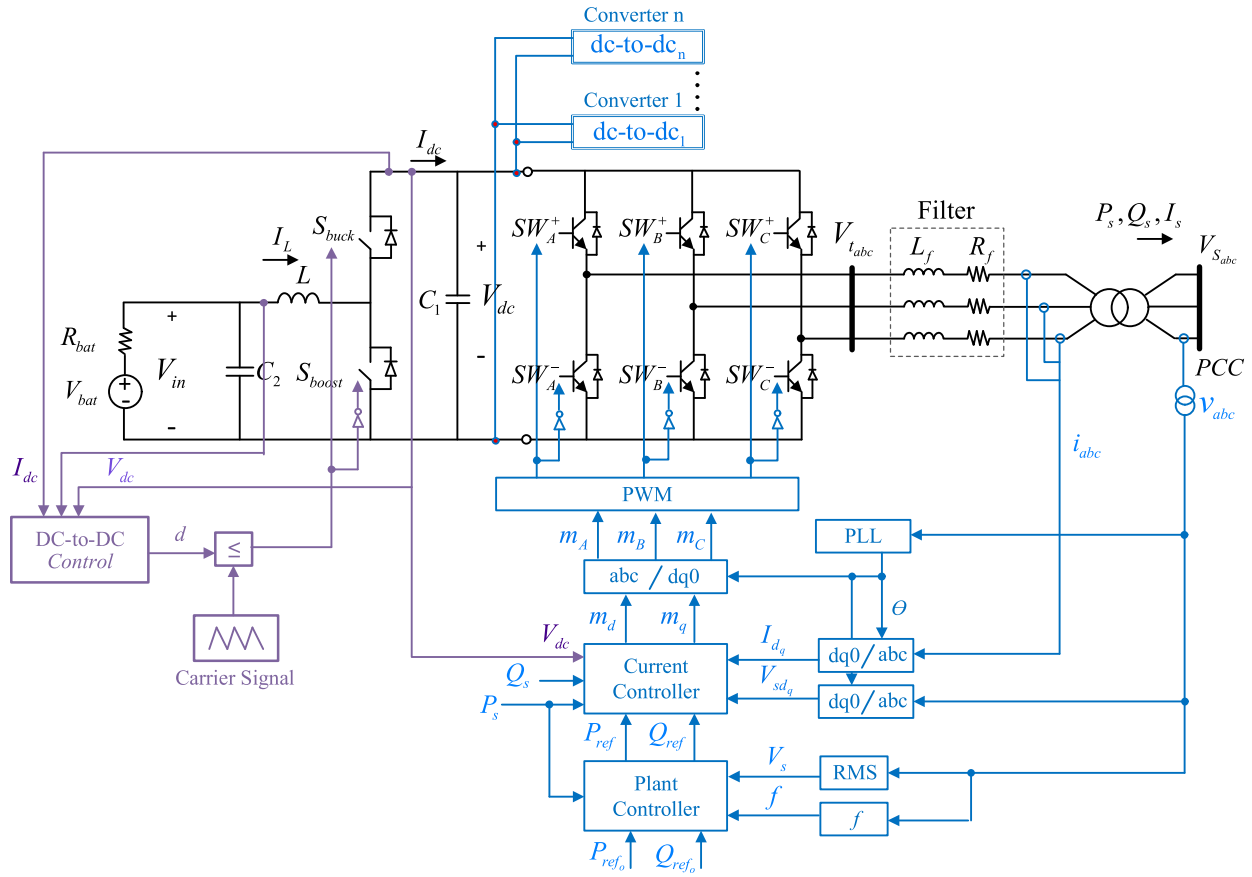


**Fig. 7.** Detailed three-phase BESS model with its generalized controls, for dynamic analysis.

significant impact on a CAES system performance during fast transient events [45]. Therefore, the CAES model discussed in this section assumes [30] the following:

- 1) a steady-flow process within the compressor and turbine, ideal gas behavior, and neglect kinetic and potential energy during compression and expansion;
- 2) a diabatic CAES system, i.e., gas is burned to preheat the air before expansion;
- 3) a very small proportion of gas to air in the expander;
- 4) constant efficiencies in all elements;
- 5) independent generation and expansion drivetrains.

In Fig. 4(b), the mechanical power  $P_{t,k}$  produced in a stage of expansion  $k = \{\text{LP, HP}\}$  of a multistage turbine, and consumed power  $P_{c,j}$  in a stage of compression  $j = \{1, 2, 3, 4\}$  of a multistage compressor of diabatic CAES, can be calculated based on the isentropic expansion/compression of the air as follows [30]:

$$P_{t,k} = \eta_{t,k}^m \eta_{t,k}^i c_p T_{t,k}^{\text{in}} \left(1 - \pi_{t,k}^{1/\gamma-1}\right) \dot{m}_t \quad (13)$$

$$P_{c,j} = \frac{c_p T_{c,j}^{\text{in}}}{\eta_{c,j}^m \eta_{c,j}^i} \left(\pi_{c,j}^{1-1/\gamma} - 1\right) \dot{m}_c \quad (14)$$

where  $\dot{m}_t$  and  $\dot{m}_c$  are the turbine and compressor air flows, respectively;  $\eta_{t,k}^m$  and  $\eta_{c,j}^m$ , and  $\eta_{t,k}^i$  and  $\eta_{c,j}^i$  are the mechanical and isentropic efficiencies of the turbine

and compressor, respectively;  $T_{t,k}^{\text{in}}$  and  $T_{c,j}^{\text{in}}$  are the air temperatures at the inlet of the turbine and compressor, respectively;  $c_p$  is the specific heat gain of air; and  $\pi_{t,k}$  and  $\pi_{c,j}$  are the turbine and compressor pressure ratios, respectively, which are functions of air flow, rotor speed, and inlet conditions, i.e., temperature and pressure. The thermal dynamics of the recuperator shown in Fig. 8(a) can be modeled as a first-order system as follows [30]:

$$\dot{v}_r = \frac{1}{\tau_R} [\epsilon_r (T_{t,\text{LP}}^{\text{out}} - T_s) - v_r] \quad (15)$$

$$T_{b,\text{HP}} = T_s + v_r \quad (16)$$

where  $\epsilon_r$  and  $\tau_R$  are the effectiveness and time constant of the recuperator, respectively,  $v_r$  is the dynamic temperature rise in the recuperator,  $T_s$  is the cavern temperature,  $T_{t,\text{LP}}^{\text{out}}$  is the exhaust temperature of the LP turbine stage, and  $T_{b,\text{HP}}$  is the input temperature to the HP burner. The relation between the burner temperature and turbine input temperature can be expressed as follows:

$$T_{t,k}^{\text{in}} = T_{b,k} + (T_{\text{to},k}^{\text{in}} - T_{\text{bo},k}) \frac{\dot{m}_f}{\dot{m}_t} \quad (17)$$

where  $(T_{\text{to},k}^{\text{in}} - T_{\text{bo},k})$  is the design burner rise temperature and  $\dot{m}_f$  is the fuel flow into the burner. The thermal

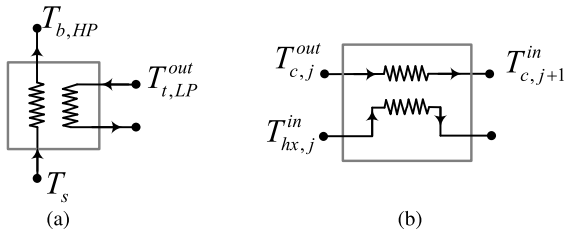


**Fig. 8. CAES component-level thermal dynamic models for (a) recuperator and (b) intercooler.**

dynamics of the intercoolers at each compression stage, shown in Fig. 8(b), can be modeled as a first-order system as follows:

$$\dot{v}_{hx,j} = \frac{1}{\tau_{hx}} \left[ \epsilon_j \left( T_{c,j}^{out} - T_{hx,j}^{in} \right) - v_{hx,j} \right] \quad (18)$$

$$T_{c,j+1}^{in} = T_{c,j}^{out} - v_{hx,j} \quad (19)$$

where  $v_{hx,j}$  and  $\tau_{hx}$  are the intercooler temperature drop and time constant, respectively. Finally, the turbine and compressor output temperatures at each stage,  $T_{t,k}^{out}$  and  $T_{c,j}^{out}$ , respectively, can be calculated as follows:

$$T_{t,k}^{out} = T_{t,k}^{in} \left[ 1 - \left( 1 - \pi_{t,j}^{1/\gamma-1} \right) \eta_{t,k}^i \right] \quad (20)$$

$$T_{c,j}^{out} = T_{c,j}^{in} \left[ 1 + \left( \pi_{c,j}^{1-1/\gamma} - 1 \right) \frac{1}{\eta_{c,j}^i} \right]. \quad (21)$$

To complete the model, synchronous machines that couple the turbine and compressor to the grid and their controls must be represented. These models are well defined in the literature, as, for example, in [46] and [47].

**3) Flywheel Energy Storage System:** A detailed FESS model based on an IM and a back-to-back configuration is presented in Fig. 9. The same model assumptions discussed for the BESS' power conditioning systems apply for the FESS, i.e., detailed three-phase physical-based or balanced average models of the FESS can be considered depending on the application, with average models being more common for large power system dynamic studies. The model of the VSCs is similar to that discussed for the BESS in Section III-A1, while typical transient IM models are readily available, e.g., [46], [47]. VSC<sub>1</sub> connected to the terminals of the IM can be controlled to regulate the active power exchanged with the flywheel and, thus, the charging and discharging of the FESS. The electromechanical coupling between the flywheel and the IM can be calculated as follows [46]:

$$\dot{\omega}_r = \frac{1}{J_{IM} + J_M} (\mathcal{T}_e - F\omega_r) \quad (22)$$

where  $\mathcal{T}_e$  is the IM electromagnetic torque,  $\omega_r$  is the rotor speed, and  $F$  is a friction coefficient. The electromagnetic torque depends on the IM stator currents and thus on VSC<sub>1</sub>'s  $I_d$  and  $I_q$  currents, which are regulated by the

current controller. Note that the sign of  $\mathcal{T}_e$  depends on the direction of the active power flow to the flywheel, i.e., it is positive if the flywheel is charging and negative if it is discharging. Similarly, from (1), the useful energy stored in an FESS can be determined as follows:

$$E = \frac{J_{FW} + J_M}{2} (\omega_r^2 - \omega_{r,\min}^2) \quad (23)$$

where  $\omega_{r,\min}$  is the minimum rotational speed of the flywheel.

**4) Thermal Energy Storage System:** The heat storage model depends on the physical characteristics of the storage reservoir. For example, a simple model is that of a tank storing a fluid such as water, whose temperature can be calculated as follows [36]:

$$m_s c_w \dot{T}_s = \dot{Q}_s^{in} - \dot{Q}_s^{out} - \dot{Q}_s^L \quad (24)$$

where  $m_s$  is the mass of water in the tank,  $T_s$  is the water temperature in the tank,  $c_w$  is the specific heat capacity of water,  $\dot{Q}_s^{in}$  and  $\dot{Q}_s^{out}$  are the heat rates for water entering and leaving the tank, respectively, and  $\dot{Q}_s^L$  represents the rate of heat loss. Note that  $\dot{Q}_s^{in}$  and  $\dot{Q}_s^{out}$  depend on the thermal loops of the TESS. This model assumes that the water density and temperature are uniform in the tank, with no phase changes in the water and neglecting pressure dynamics [48]. Due to these assumptions, the application of this model results in fast computation times, and it is thus extensively used in operation and planning studies or when multiple TESSs need to be modeled. However, the model is not accurate enough to reflect effects such as thermal stratification inside the TES, and it thus tends to overestimate heating losses [49].

In the specific case of the GSHP system shown in Fig. 6,  $\dot{Q}_s^{in}$  when the GSHP operates in cooling mode, i.e., replacing an A/C in the household, can be obtained by following the thermal loops and observing the heat transfers and energy conversion processes. For example, the cooling power  $\dot{Q}_c$  can be calculated as a function of the wet-bulb house temperature  $T_{wb}$ , the mass flow rate in the borehole loop  $\dot{m}_w$ , and the water temperature at the inlet of the heat pump, i.e., borehole temperature  $T_s$ , as follows [38]:

$$\frac{\dot{Q}_c}{\dot{Q}_{c,\text{ref}}} = \mathcal{A} + \mathcal{B} \left( \frac{T_s}{T_{\text{ref}}} \right) + \mathcal{C} \left( \frac{T_{\text{ref}}}{T_{wb}} \right) \left( \frac{\dot{m}_w}{\dot{m}_{w,\text{ref}}} \right) \quad (25)$$

where  $\mathcal{A}$ ,  $\mathcal{B}$ , and  $\mathcal{C}$  are model parameters that can be obtained from actual systems,  $T_{\text{ref}}$  is a reference temperature (283 °K),  $\dot{m}_{w,\text{ref}}$  is the reference mass flow rate, and  $\dot{Q}_{c,\text{ref}}$  is the rated cooling capacity of the heat pump. Thus, the compressor power  $P_c$  can be computed as follows [38]:

$$P_c = \frac{\dot{Q}_c}{\text{ERR}} \quad (26)$$

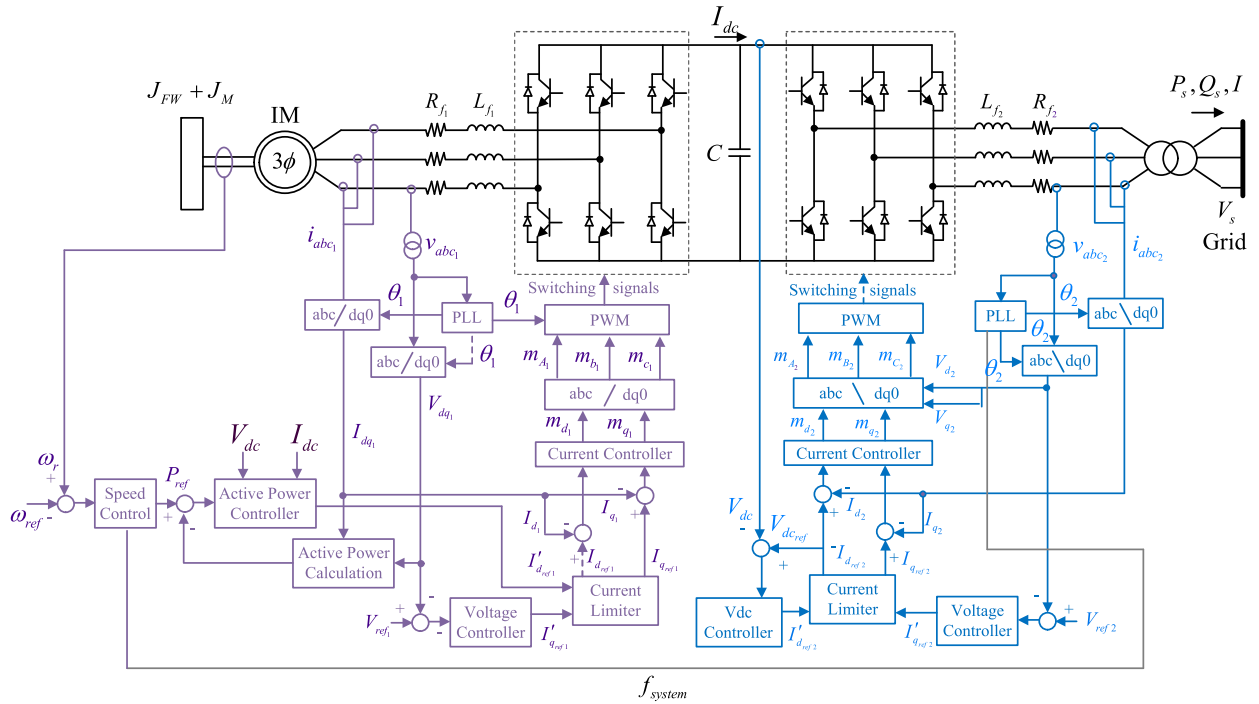


**Fig. 9.** Detailed FESS model based on an IM and a back-to-back converter configuration, with its generalized controls for dynamic analysis.

$$\frac{\text{ERR}}{\text{ERR}_{\text{ref}}} = \mathcal{D} + \mathcal{E} \left( \frac{T_s}{T_{\text{ref}}} \right) + \mathcal{F} \left( \frac{T_{\text{ref}}}{T_{\text{wb}}} \right) \left( \frac{\dot{m}_w}{\dot{m}_{w,\text{ref}}} \right) \quad (27)$$

where EER and EER<sub>ref</sub> are the actual and rated efficiency ratios of the heat pump, respectively, and  $\mathcal{D}$ ,  $\mathcal{E}$ , and  $\mathcal{F}$  are model parameters that can be obtained from actual deployed systems. The heat power rejected to the ground  $\dot{Q}_s^{\text{in}}$  and the heat pump outlet water temperature  $T_w^{\text{out}}$  can be calculated as follows:

$$\dot{Q}_s^{\text{in}} = \dot{Q}_c + P_c \quad (28)$$

$$T_w^{\text{out}} = \frac{\dot{Q}_s^{\text{in}}}{c_p \dot{m}_w} + T_s. \quad (29)$$

To model the GSHP in heating mode, the parameter EER is replaced by the coefficient of performance COP =  $\dot{Q}_c/P_c$ ,  $T_{\text{wb}}$  is replaced by the dry-bulb indoor temperature, and (28) and (29) are reformulated as follows:

$$\dot{Q}_s^{\text{out}} = \dot{Q}_c - P_c \quad (30)$$

$$T_w^{\text{out}} = \frac{\dot{Q}_s^{\text{out}}}{c_p \dot{m}_w} - T_s \quad (31)$$

where  $\dot{Q}_s^{\text{out}}$  is the heat extracted from the borehole. Note that this model assumes that the COP is constant. For shorter term studies, such as using the TESS for frequency control, a more complex model than (24) should be used to describe the borehole, such as the one, for example, in [38], which is able to accurately reproduce the dynamic

behavior of the ground heat exchange under transient operating conditions (ON/OFF operations) for cooling and heating modes.

## B. Control Strategies

1) *Battery Energy Storage System:* In most grid-connected BESS, the VSC can be controlled to regulate the active and reactive power injections, while the dc-to-dc converter regulates the dc-link voltage. An alternative to this approach involves regulating the dc-link voltage and  $Q$  injections along with the VSC and the active power by means of the dc-to-dc converter. In either case, a decoupled  $dq$  current controller facilitates independent control of  $P$  and  $Q$  services.

A two-level hierarchical control strategy for BESS is presented in Fig. 10 [50]. In the first level, known as plant controller, the set points of the BESS active and reactive power injections are calculated and split into  $N_c$  modules in the second level, each comprising a VSC, its current controller, and  $M_c$  dc-to-dc converter per VSC. The active power plant controller allows the BESS to provide OD, PFR, and SFR to operate in constant  $P$  mode following an external reference signal,  $P_{\text{ref},o}$ , or a combination of these. Similarly, the reactive power plant controller allows voltage regulation, constant power factor operation, or constant  $Q$  control following an external reference signal  $Q_{\text{ref},o}$ . To choose between different operating modes, two flags are used. The dc-to-dc converter controls the  $S_{\text{boost}}$  and  $S_{\text{buck}}$  switches in Fig. 7 while keeping the current through

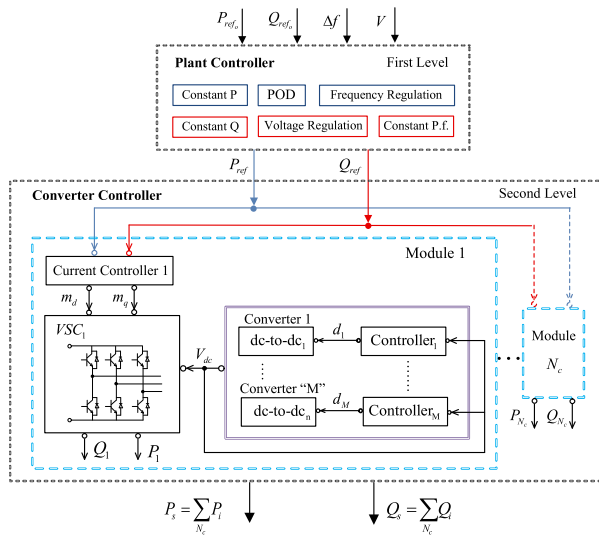


Fig. 10. Two-level hierarchical control of BESS [50].

the dc converter inductor  $L$  within limits, thus also limiting the battery bank charge and discharge.

Another BESS model widely used in the industry, which was developed by the WECC, based on a generic renewable generator model, is the so-called WECC BESS model [51]. It comprises three modules: energy converter model (REGC\_A), electrical control model (REEC\_C), and plant controller (REPC\_A). The current control for the VSC is modeled in the REPC\_A, which allows the BESS to provide frequency regulation, constant  $PQ$  control, constant power factor control, and voltage regulation with droop. Also, a current control limiter is incorporated in REPC\_A, which prevents the BESS from operating overloaded by limiting the current that can be drawn from the VSC, whereas an SoC logic control limits the current if the battery is completely charged or discharged. In [52], modules REGC\_A, REEC\_C, and REPC\_A are updated with more accurate modules REGC\_C, REEC\_D, and REPC\_C, respectively.

**2) Compressed Air Energy Storage :** A general scheme of the control system for a diabatic CAES is presented in Fig. 11, based on [45]. The active power control in the turbine is achieved by varying the air flow, using a valve whose cross-sectional area is represented by  $\lambda$ , i.e., when  $\lambda = 1$ , the valve is fully open, and when  $\lambda = 0$ , the valve is fully closed. The temperature in the burners is regulated by adjusting the amount of fuel injected into the fuel flow system  $y$ , aiming to keep the expansion temperature constant and thus increasing the system efficiency.

The IGVs of the first compression stage can be used to regulate the air flow through the compressor and, thus, its mechanical power. Additional control systems are necessary to prevent compressor surge and regulate the output pressure by limiting the air flow. As in other storage technologies, an SoC limit control can be used to track the

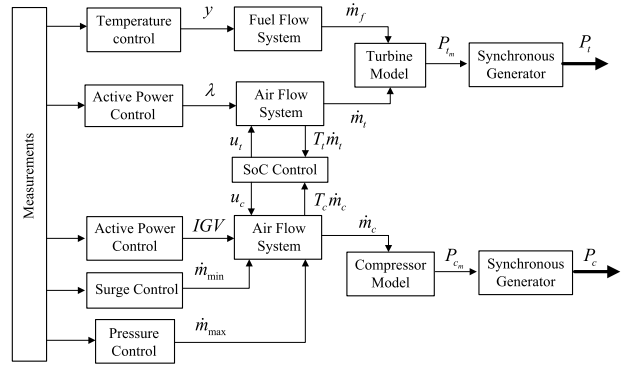


Fig. 11. CAES control system architecture [30].

SoC, which, in CAES, is directly related to the cavern pressure. Finally, when considering two independent machines, a coordinated droop-based control would allow CAES to provide frequency regulation, reactive power with its two synchronous machines (motor and generator) connected at the same bus while distributing the active and reactive power between the machines as a function of their loading.

**3) Flywheel Energy Storage System :** The grid-side VSC can be controlled to regulate the PCC voltage and the dc-side voltage by independently controlling the reactive and active power injected, which can be achieved with a decoupled  $dq$  current controller, as in BESS and shown in Fig. 9. On the other hand, the flywheel side converter can be controlled to regulate the active power exchanged with the flywheel as well as the IM terminal voltage. The speed control for the IM-side converter control limits the maximum and minimum rotational speed of the flywheel and, thus, its SoC and allows the provision of frequency regulation by a PID controller [39], which uses the measured system frequency  $f_{sys}$  as input, as shown in Fig. 12. The output of this controller is the power reference  $P_{ref}$  in Fig. 9, which is then compared to a calculated active power based on  $I_{dc}$  and  $V_{dc}$  and the error passed through a PI regulator that yields  $I_{d_{ref1}}$  fed to the current controller.

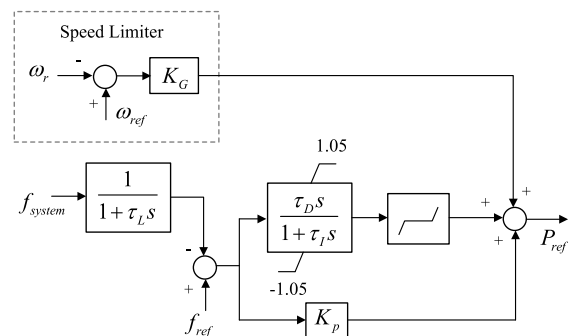


Fig. 12. FESS speed control [53].

On the other hand, the measured IM terminal voltage can be used in a PI-based voltage controller, which yields  $I_{q_{\text{ref}_1}}$ . In the grid-side converter, the measured dc link is compared to a reference value and the error is passed through a PI controller ( $V_{\text{dc}}$  controller), which yields  $I_{d_{\text{ref}_2}}$ , while the terminal voltage at the PCC is regulated by another PI (voltage controller) that controls  $I_{q_2}$ .

Another common control strategy for the IM-side converter  $\text{VSC}_1$  is the flux-oriented control, in which the  $dq$  reference frame is locked to the rotor flux, i.e.,  $\psi_{r_q} = 0$ , thus allowing independent rotor flux and torque control, by controlling  $I_{d_1}$  and  $I_{q_1}$ , respectively, given as follows [54], [55]:

$$I_{q_{\text{ref}_1}} = \frac{\mathcal{T}_{\text{ref}} L_r}{M \psi_{\text{ref}}} \quad (32)$$

$$\psi_{\text{ref}} = \frac{P_e L_r}{M I_{q_{\text{max}_1}}} \quad (33)$$

$$I_{d_{\text{ref}_1}} = h(\psi_{\text{ref}} - \psi_{r_d}) \quad (34)$$

where the reference current  $I_{q_{\text{ref}_1}}$  is a function of the desired torque flux  $\psi_{\text{ref}}$ ,  $\mathcal{T}_{\text{ref}}$  is the electromagnetic torque,  $M$  is the mutual inductance,  $L_r$  is the rotor inductance,  $P_e$  is the electrical power, and the reference current  $I_{d_{\text{ref}_1}}$  is obtained as output of a controller represented by the function  $h$ , which has the rotor flux error  $\psi_{r_d}$  as input. These reference currents are then passed through current controllers, which ultimately defines the modulating signals to control the switches of the IM-side VSC.

*4) Thermal Energy Storage System :* The control strategies for TESS involve regulating the heat injections to the thermal storage element to achieve the desired objective. For example, the power exchanged with the electrical grid by a GSHP can be controlled to provide frequency regulation by switching its compressor ON/OFF while satisfying the thermal needs of the house [38].

In an MG, on the other hand, where multiple independent heat sources may be available such as solar collectors, boilers, or heat as subproduct of other processes (e.g., the remnant heat from thermal generators), an EMS can be developed to coordinate the operation of all these energy resources. For example, for the MG shown in Fig. 13, the discrete-time version of (24), which models the storage tank, can be expressed as follows [36]:

$$m_s c_w \left( \frac{T_{s,t} - T_{s,t-1}}{3600 \Delta t_t} \right) = \dot{Q}_{s,t}^{\text{in}} - \dot{Q}_{s,t}^{\text{out}} - \dot{Q}_t^L \quad (35)$$

$$\dot{Q}_{s,t}^{\text{in}} = \sum_{g \in G} \dot{Q}_{g,t}^u + \sum_{j \in J} \dot{Q}_{j,t}^B \quad (36)$$

where  $t$  is a time step index,  $T_s$  is the water temperature,  $m_s$  is the mass of the water in TSS,  $c_w$  is the water specific heat,  $\Delta t_t$  is the time interval between  $t$  and  $t+1$ ,  $\dot{Q}_{s,t}^{\text{in}}$  and  $\dot{Q}_{s,t}^{\text{out}}$  are the thermal power injected and extracted from the tank at period  $t$ , respectively,  $\dot{Q}_{g,t}^u$  is the usable heat

power produced in the generator  $g$ ,  $\dot{Q}_{j,t}^B$  is the thermal power from boiler  $j$ , and  $\dot{Q}_t^L$  is the thermal losses of the TESS. This model can be readily integrated in an EMS to keep track of the thermal storage element, also defining temperature limits for its safe operation, i.e.,  $T_s^{\min} \leq T_{s,t} \leq T_s^{\max}$ . Note that  $\dot{Q}_{s,t}^{\text{in}}$  in (36) can be modified to include the heat from other sources, such as solar collectors, while  $\dot{Q}_{s,t}^{\text{out}}$  depends on the objective sought by the EMS, such as to control the import/export from the main grid, minimize losses, maximize the use of renewables, and minimize fuel costs, among others [37]. Furthermore, an EMS such as the one shown in Fig. 13 could improve the efficiency of the MG energy supply, considering that remnant heat from CHP units, TESSs, or boilers can be used to supply the heating/cooling needs, thus replacing A/C or grid-connected HPs when it is economical to do so.

If a GSHP supplies a part of the thermal demand of a building in an MG, the heat power injected,  $\dot{Q}_{\text{HP}}$ , if it operates in heating mode, can be modeled based on its COP, and (24) and (30), which is given as follows [39]:

$$\dot{Q}_{\text{HP}} = c_w m_w (T_{w,t}^{\text{in}} - T_{w,t}^{\text{out}}) + P_{c,t} \text{COP} \quad (37)$$

where  $T_{w,t}^{\text{in}}$  and  $T_{w,t}^{\text{out}}$  are the inlet and outlet water temperatures in the borehole terminals at period  $t$ , respectively,  $m_w$  is the mass of water, and  $P_{c,t}$  is the power consumed by the heat pump. The first term in (37) represents the heat obtained from the borehole, whereas the second is the heat added by the compressor.

## C. Aggregated Models

Existing computing capabilities can handle large and complex models and simulations with relative ease, which was not possible in the past; however, detailed modeling of distribution systems connected to transmission systems is still computationally challenging. On the other hand, the trend in ESS, particularly BESS and TESS, indicates that many new deployments will be at the distribution level, rather than large utility-scale ESS at the transmission level. Hence, aggregation of ESSs is an important topic to consider when modeling and simulating power systems. Aggregation of DERs typically involves developing gray- or black-box models, which can either represent a portion of the power grid or the aggregated response at the aggregating point of a group of DERs. However, black-box models are more advantageous than gray-box models in which the former do not require knowledge of the grid topology or its components and are capable of representing highly nonlinear behavior; nevertheless, these are data-intensive models that require a training stage. For example, in Fig. 14, an NN-based black-box model to aggregate the BESSs in ADNs is depicted. This model, which comprises an NN for the aggregated BESS  $P$  injections at the boundary bus between the ADN and the transmission system, and another for  $Q$ , assumes that the BESSs are controlled to provide upstream grid services,

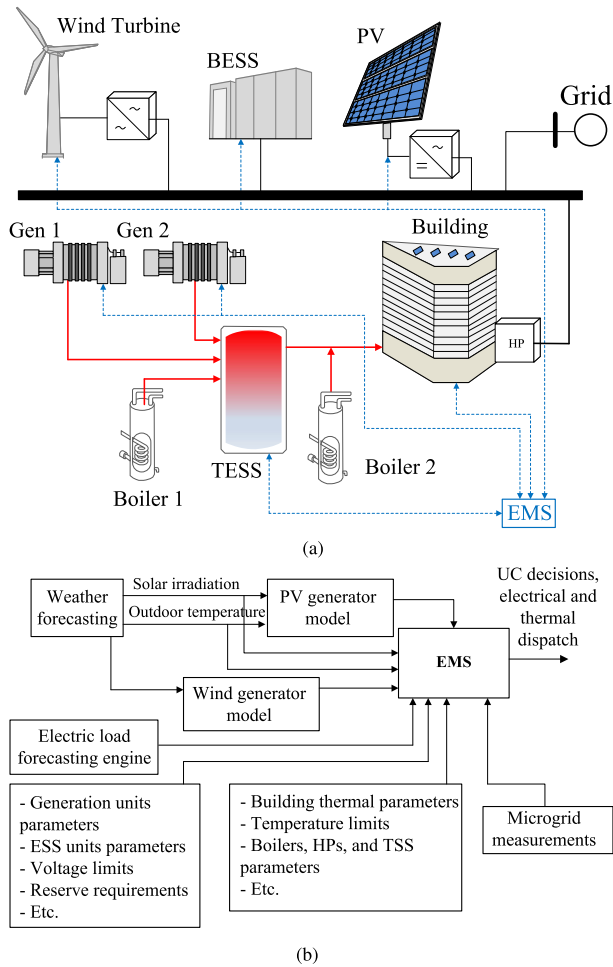


**Fig. 13.** Typical MG configuration with (a) hot water-based TESS and (b) its corresponding EMS [36].

such as frequency regulation, local voltage regulation, and OD. This model aggregates the active and reactive BESS power injections  $P$  and  $Q$ , respectively, using two NARX NNs. These NNs can be trained with simulation or measurement data of  $V$ ,  $f$ , and PV at the boundary bus, with the latter being proportional to the solar irradiance, thus allowing capturing the effects of distributed PV generation on the BESS response, and the external control signals  $P_{ref}$  that directly modifies the BESS set points. The topology of the black-box model, i.e., the number of neurons per hidden layer, is obtained as the solution of an optimization procedure that seeks to minimize the validation error of the model with respect to measurements obtained for some contingencies using a GA [56].

#### D. ESS for Frequency Regulation in Large Power Systems

Power systems require a continuous balance between generation and load to safely operate without any mismatch causing the system frequency to deviate from its nominal value and affecting some frequency-sensitive

loads such as motors. The generation-load unbalance is especially damaging for thermal units such as steam units, whose mechanical components can suffer excessive cumulative stress when their turbines operate at frequencies different from the nominal, requiring special protection equipment that may trip these units, and this results in system stability problems. The control actions performed by generating units to adjust their output power in response to frequency deviations are called frequency regulation.

After a disturbance, most generating units automatically adjust their output power through a local proportional controller that receives a speed deviation feedback, known as PFC, whose objective is to stabilize the system frequency at a value different from the nominal, with all units contributing in proportion to their governor droop rates. Some generators, which operate in AGC, receive signals from the ISO to further adjust their power references to bring the system frequency back to its nominal value, which is referred to as SFC. In large interconnected power systems, generation-load mismatches could also affect the scheduled power flows through the tie lines. Thus, a special control signal synthesized from the deviations in tie line flow and frequency, known as ACE, is determined by the ISO and fed to the units on AGC, aiming to keep the ACE within acceptable limits.

In Ontario, Canada, the IESO has contracts with hydro and gas units, and ESSs to provide regulation services, for a minimum of  $\pm 100$  MW at a ramp rate of  $\pm 50$  MW/min every hour [57]. In 2012, ESS participation was procured under the IESO's ATR initiative, which contracted a total of 6 MW of storage in two projects: BESS and FESS. Later, in 2014, a competitive energy storage procurement framework expanded this capacity by another 50 MW, including CAES. Most of these storage units receive regulation signals by the IESO, which they must follow.

A model to study the frequency regulation, considering the participation of fast ESS units such as BESS and FESS, is shown in Fig. 15 [58]. Such a model allows

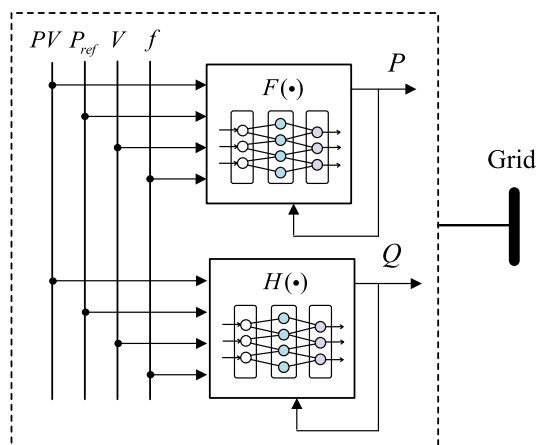


**Fig. 14.** Black-box aggregated model of BESS [56].

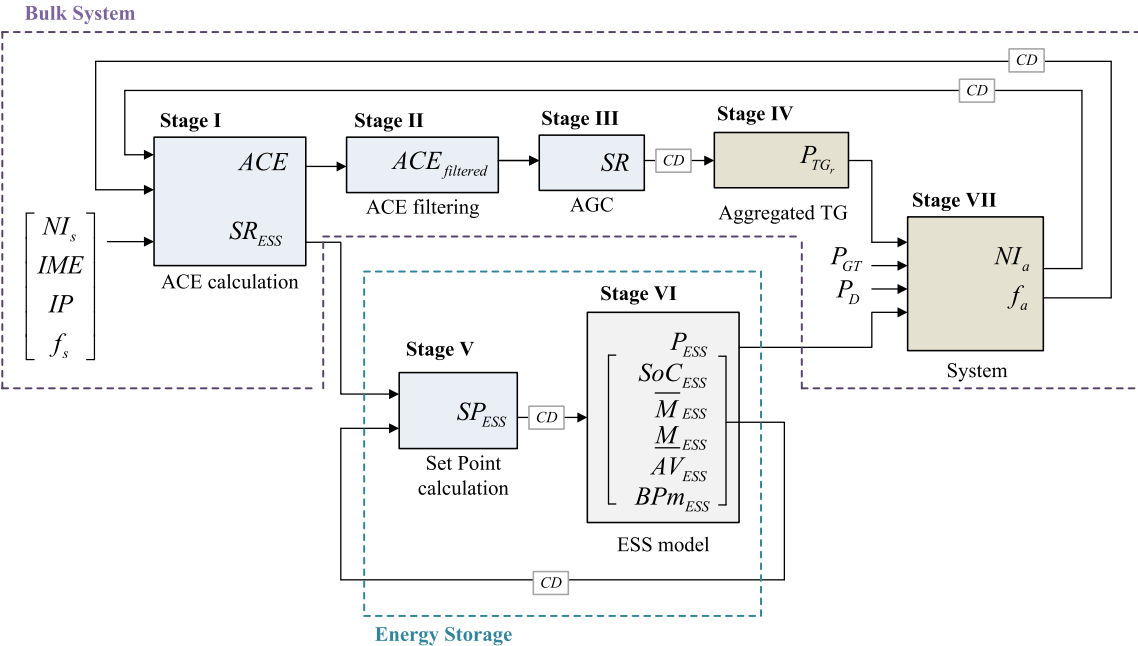


Fig. 15. Frequency response model of large interconnected power systems with ESS [58].

performing long-term frequency studies and helps in tuning the ACE calculation and filtering without the need of modeling the entire electrical grid. The model is divided into seven stages. Stage I corresponds to the ACE block, which compares the actual and scheduled power in the interconnection  $NI_a$  and  $NI_s$ , respectively, and the actual and scheduled system frequency  $f_a$  and  $f_s$ , respectively, to calculate the ACE signal sent to the TGs contracted for regulation and a signal  $SR_{ESS}$  sent to the ESSs based on the bias factor  $B$ . The complementary signals IME and IP representing metering errors and inadvertent payback, respectively, adjust the ACE. Stage II filters out fast ACE changes before being sent to the TGs, and Stage III models the AGC, which is a PI controller with antiwindup, a rate limiter (e.g.,  $\pm 50$  MW/min in Ontario), and a saturation block to limit the regulation capacity (e.g.,  $\pm 100$  MW in Ontario). Stage IV models the aggregated TG response, Stage V calculates the ESS set points based on the  $SR_{ESS}$  signal, and Stage VI models the ESS. Finally, Stage VII corresponds to a model of the primary frequency response of the system, which considers the load of the system, generation total dispatch, and outputs of the TGs and ESSs contracted for frequency regulation. One major challenge faced by large interconnected systems, such as the Ontario system, is the communication delays between the IESO and the regulating facilities, represented by the blocks CD in the figure. These delays can significantly impact the performance of the system frequency regulation, particularly worsening the ACE signal if they are not properly accounted for.

A further improvement of the model in Fig. 15 consists of replacing Stages II and III by a filter, to split the ACE signal into a fast component ( $SREG_D$ ), which is sent to

fast response units such as BESS or FESS and slower component ( $SREG_A$ ) sent to slower assets such as TGs or CAES. Also, Stage V can be modified to take advantage of the fast  $SREG_D$  signal when defining the operating point of the ESSs [59].

## E. Behind-the-Meter CAES

For small-scale CAES owned by customers and connected behind-the-meter, the system operation model proposed in [60] minimizes the electricity cost and CAES operation cost of the customer. The optimization problem considers a given small-scale CAES facility to determine its optimal charging/discharging decisions and energy purchase/consumption schedules of the customer. In the model, the base case cost of the customer considers an EnC and demand charges, i.e., the GAD in Ontario. In particular, the CAES is arranged to shave the demand during the top five Ontario peak load hours, referred to as five coincident peak (or 5 cp) hours and also to reduce the energy drawn from the grid. The CAES power/energy rating is considered feasible if the total cost of the customer with CAES is lower than its total cost without CAES, which is given by

$$TC^{No\ CAES} = EC^{NoCAES} + GAD^{NoCAES} \quad (38)$$

where  $EC^{NoCAES}$  is the cost of energy consumed by the customer over one year at the corresponding energy price. The component  $GAD^{NoCAES}$  considers the customer's contribution to the 5-cp hours. On the other hand, the total annual electricity bill savings obtained by deploying the CAES facility is determined using the optimization model

to minimize the total annual cost of the customer, which is given by

$$TC^{CAES} = EC^{CAES} + GAD^{CAES} + SVOMC + SFOMC \quad (39)$$

where the variable operation and maintenance (O&M) cost (VOMC) during the charging/discharging operation of the CAES facility is represented by SVOMC and the annual fixed O&M cost (FOMC) per year is given by SFOMC. According to [60], an appropriate general starting point for the FOMC is between 1% and 1.5% of the capital cost.

## F. Ground Source Heat Pump

A thermal load aggregation approach to minimize an aggregator's energy procurement cost is proposed in [39] and [61]. This model considers the GSHP characteristics to optimize the electricity usage by end users while considering household thermal comfort. The model aggregates the information of the uncontrolled loads in the house, the house thermal and heating system characteristics, and the current and forecast ambient temperatures, which are used to optimally schedule the heating load of each house in order to minimize its total electricity cost. Two stages for the purchase of energy are considered, i.e., DA and RT markets.

In the first DA stage, the aggregator participates considering a forecast market price for the next day  $\lambda_t^{DA}$  while minimizing the following total electricity cost to determine the thermal load of the house that satisfies a required in-house temperature comfort range:

$$J_1 = \sum_t^T \lambda_t^{DA} P_t^{DA}. \quad (40)$$

Accordingly, hourly demand bids are submitted to the wholesale electricity market to serve the scheduled load for 24 h of the next day. In the RT stage, the aggregator's objective is to minimize the penalty payable for any deviations in RT load dispatch from the DA dispatch, at the RT market price, defined by

$$J_2 = \sum_t^T \lambda_t^{RT} |P_t^{DA*} - P_t^{RT}|. \quad (41)$$

Both market models contemplate constraints related to the total load that the aggregator will procure at a specific hour, thermal power consumption, in-house temperature levels for an end user's comfort range, cycling constraints, power consumption of the GSHP, and in-house and external wall temperatures.

## G. Integration of ESS in Electricity Markets

Market participation models for ESS must consider their special operational characteristics that differentiate them from other market participants' loads and generators,

such as the ability to charge/discharge, fast ramp rates, cycling limitations, and their energy and power dependence. These aspects need to be properly reflected in the cost structure of the ESSs and hence in their bids/offers; consequently, operational models for each specific ESS technology are needed. Likewise, the market structure should be adapted to allow participation of ESSs in the wholesale energy market, capacity market, and ancillary service market in a fair and competitive manner, with the latter being particularly relevant for fast response ESSs, such as BESSs and FESSs. For example, in the USA, the NYSO, PJM, CAISO, and ISO New England have already implemented some market design changes to allow ESS participation to comply with FERC Order 841 [62]. Depending on the ESS capacity compared to the overall system, its participation strategy may change, operating as a price taker if small or as a price maker if large.

In North America, motivated by the FERC Orders 841 and 755 [63], [64], some ISOs and RTOs have implemented a mechanism that remunerates market participants that provide frequency regulation services based on their performance and considering [65]: the capacity that they can offer at a given period; the "mileage," defined as the sum of the absolute value of the regulation signal they have to follow over a given period; and a performance factor, which measures how close the facility follows the regulation signal. This mechanism aims to promote the participation of fast regulation assets, such as ESSs, which are characterized for having large ramping rates and very fast response. To further incentivize ESSs participation, some markets have split the regulation signal into fast and slow, with the former receiving higher compensation for being followed.

In the existing market frameworks that allow ESSs, particularly BESS, to participate, the bids/offers do not explicitly represent degradation, discharge rates, or SoC; however, BESS operational costs, including degradation costs based on their DoD and discharge rate, should be considered [62]. In such markets, BESS can participate in electricity markets as loads or generators, being able to submit bids to charge and offers to discharge, while reflecting their marginal operating costs. BESS may also participate in reserve markets by providing its capacity in the form of a discharge offer. In such a market model, the operation cost of a BESS is comprised of the following components.

- 1) A degradation cost based on DoD and discharge rate. A relevant aspect in this cost is considering into the DoD the impact of SoC starting and ending levels. To model this, the ISO-monitored energy level should be considered, where the SoC and lower/upper storage limits of the ESS are available to the ISO, to ensure that the facility's schedules in the DA and RT markets are feasible within their operating limits.
- 2) High charging and discharging currents expressed by the discharge rate of a battery, as these contribute to BESS degradation.

Therefore, the BESS operational cost that can be integrated into a market model is based on the DoD and discharge rate of the facility. A second component of the cost is related to the SR capability in the SR market. The opportunity cost of not participating in energy-only markets can be attributed to the SR cost of BESS, which could be determined as the difference in revenue earning from the participation in an energy-only market and in a co-optimized energy and SR market.

A framework and mathematical model for BESS participation in an LMP based, co-optimized energy and SR market are presented in [62]. The objective is to maximize the social welfare, which includes the gross surplus of customers and BESS during charging, the total cost of generators including the generator start-up cost and shutdown cost, the cost of SR provisions from generators, and the cost of BESS for energy provisions during discharging, accounting for degradation based on DoD and discharge rate, and SR provision from the BESS during discharging.

A price-taker ESS facility participating in a DA market providing energy, spinning, and IDs, i.e.,  $Y := \{E, SR, ID\}$ , is able to operate in different modes  $X := \{C, D, SRC, SRD, ID\}$ , i.e., charging  $C$  or discharging  $D$  in the energy market, charging and discharging in the SR market SRC and SRD, respectively, and operating in idling mode ID. In this context, the owner seeks to maximize its profit  $\mathcal{F}$  as follows [66]:

$$\max_{P_t^X} \mathcal{F} = \sum_t^T \left( \sum_{X \in \mathcal{M} \setminus C} \phi_t^Y P_t^X - \phi_t^E P_t^C - OC_t \right) \quad (42)$$

where  $\phi_t^Y$  is the hourly price of the market  $Y$ ,  $P_t^X$  is the ESS power for mode  $X$ , and  $OC_t$  is the operational cost of the ESS, which includes variable operational and maintenance costs, and other costs specific to certain ESS technologies (e.g., fuel costs for CAES [66] or degradation costs for BESS [62]). This is subject to the following operational constraints:

$$P_t^C \leq \bar{P}_x^C x_t^C \quad (43)$$

$$\underline{P}_x^C x_t^C \leq P_t^C - P_t^{SRC} \quad (44)$$

$$P_t^D + P_t^{SRD} \leq \bar{P}_x^D x_t^D \quad (45)$$

$$\underline{P}_x^D x_t^D \leq P_t^D \quad (46)$$

$$0 \leq P^{ID} \leq QSC \left[ 1 - (x_t^C + x_t^D) \right] \quad (47)$$

$$x_t^C + x_t^D \leq 1 \quad (48)$$

where  $x_t^C$  and  $x_t^D$  are binary variables at time  $t$ , which are equal to 1 when the ESS charges or discharges, respectively; QSC is the quick start capacity of the ESS; and the parameters with bars above and below represent the ESS's maximum and minimum power  $P$  capacities in its different operating model  $X$ , respectively. Note that (48)

prevents the ESS facility from simultaneously charging and discharging and thus could be eliminated if, for instance, an ESS such as the CAES with such capability is considered. Furthermore, ESSs are limited by their SOC, which requires adding dynamic constraints to the model as follows [66]:

$$SOC_{t+1} = SOC_t + P_t^C \eta^C - P_t^D / \eta^D \quad (49)$$

$$\underline{SOC} \leq SOC_t \leq \overline{SOC} \quad (50)$$

where  $\eta^C$  and  $\eta^D$  are the charging and discharging efficiencies of the ESS, respectively. Even though (49) works relatively well for most ESSs, some technologies require more complex nonlinear relations that describe the conversion of electricity into another energy form to be stored. For example, the SoC for CAES can be expressed as a function of the mass flow rates as follows:

$$SOC_{t+1} = SOC_t + \frac{3,600 P_t^C AFR^C (SOC_t)}{\overline{CA}} - \frac{3,600 P_t^D AFR^D (P_t^D)}{\overline{CA}} \quad (51)$$

where  $AFR_t^C$  and  $AFR_t^D$  are the charging and discharging air flow rates, which are functions of  $SOC_t$  and  $P_t^D$ , respectively, and  $\overline{CA}$  is the cavern's air mass when it is fully charged.

To account for uncertainties, prices  $\phi_t^Y$  in the different markets  $Y$  can be expressed based on a forecast center value  $\phi_{o,t}^Y$  and a price deviation  $\Delta\phi_t^Y$  as follows [66]:

$$\phi_t^Y = \phi_{o,t}^Y (1 + \Delta\phi_t^Y) \quad (52)$$

$$\Delta\phi_t^Y = \Delta\phi_t^{Y+} - \Delta\phi_t^{Y-} \quad (53)$$

where  $\Delta\phi_t^{Y+}$  and  $\Delta\phi_t^{Y-}$  are upward and downward price deviations, respectively. By substituting (52) and (53) into (42), the objective function becomes a function of the price deviations  $\Delta\phi_t^Y$ , assuming that the forecast values  $\phi_{o,t}^Y$  are known. Thus, an RO approach, which seeks to maximize the profit and minimize the price deviation, can be used to solve the problem, with the following additional constraints:

$$0 \leq \Delta\phi_t^{Y+}; \quad \Delta\phi_t^{Y-} \leq \overline{\Delta\phi} \quad (54)$$

$$\sum_t^T \frac{\Delta\phi_t^{Y+} + \Delta\phi_t^{Y-}}{\overline{\Delta\phi}} - \Gamma \leq 0 \quad (55)$$

where  $\overline{\Delta\phi}$  is the maximum price mismatch and  $\Gamma$ , known as the budget of uncertainty, limits the number of times the prices deviate from the forecast value, thus allowing to adjust the conservatism level of the price uncertainty.

Another approach to incorporate uncertainty in the model is AA. In this case, the uncertain price is expressed

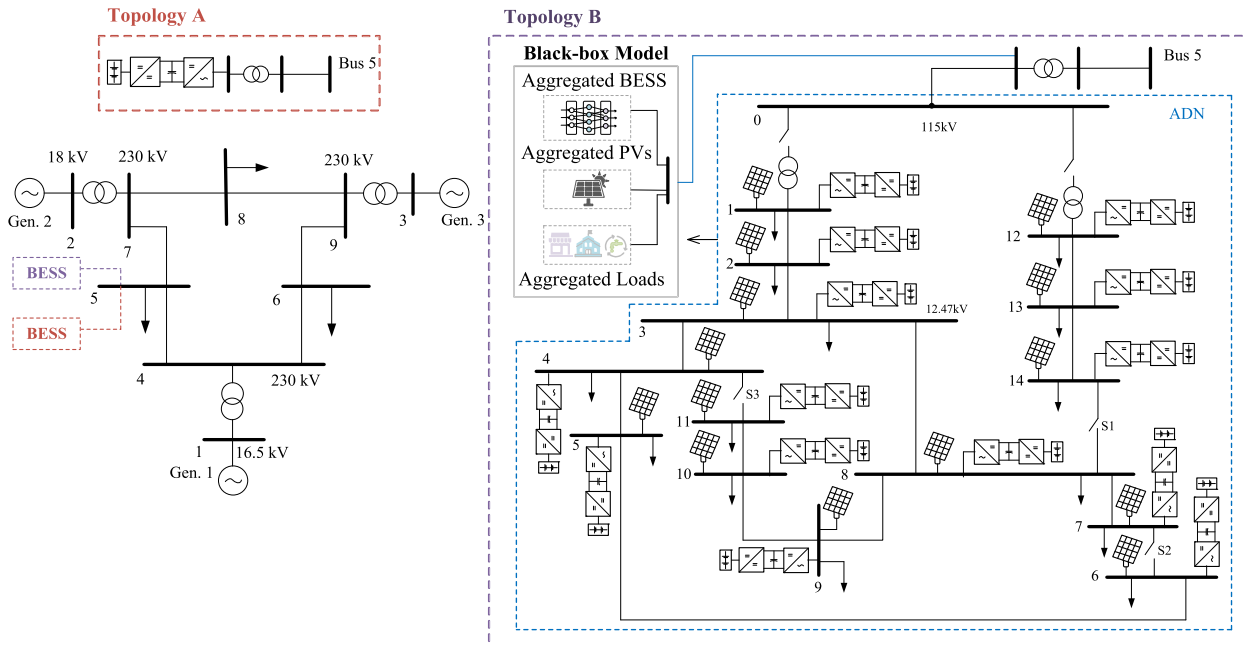


**Fig. 16.** Modified WSCC 9-bus test system for ESS grid studies.

as follows [66]:

$$\hat{\phi}_t^Y = \phi_{0,t}^Y \left( 1 + \varepsilon_t^Y \overline{\Delta\phi} \right) \quad (56)$$

where  $\phi_{0,t}^Y$  is the center value of the price and  $\varepsilon_t^Y \in [-1, 1]$  and  $\overline{\Delta\phi}$  are the noise term and magnitude of the uncertain price component, respectively. This approach requires that all model variables are expressed in their affine forms, sharing the same noise variables. This problem can be solved by maximizing the center and radius of the objective function, which has also to be expressed in its affine form, separately or simultaneously, if binary and intertemporal variables are considered in the model. A price-maker model for ESSs participating in electricity markets is discussed in [62].

#### IV. ESS APPLICATIONS AND CASE STUDIES

In this section, the most common ESS applications for transmission and distribution grids, and MGs are illustrated through simulations based on the ESS models, controls, and EMSs, discussed in Section III, and focusing on results obtained for test benchmark systems.

##### A. Frequency Regulation

Fast response ESSs, such as BESS or FESS, can significantly improve the system frequency regulation, either by following the regulation signals from the ISO in a centralized approach or acting independently based on local decentralized controls. Furthermore, given the distributed characteristics of the ESS assets, regulation services based

on properly coordinated local measurements can help address the issue of communication delays associated with a centralized approach.

1) WSCC 9-Bus Test System: The effectiveness of a grid-scale and distributed BESS connected to a transmission system to provide frequency regulation was studied on the WSCC 9-bus test system shown in Fig. 16 [56], [67]. Topology A corresponds to a bulk 45-MW BESS connected at Bus 5, and Topology B represents groups of three 1.5-MW BESSs connected at each load bus, with the latter corresponding to around 2.4% of the system installed capacity and 4% of the total system load [41]. In both topologies, the BESSs were configured to provide PFC and SFC based on local frequency measurements, while the three generators in the system provide PFC only. Fig. 17 shows the system frequency fluctuations for 20-MW

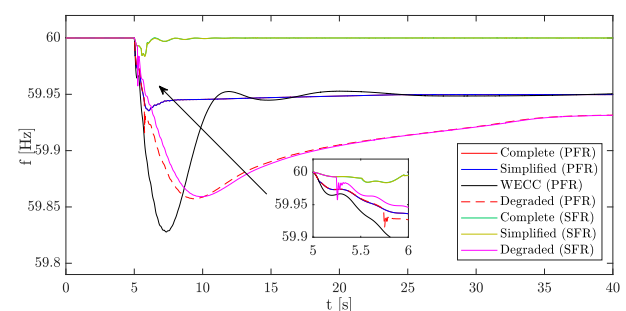


**Fig. 17.** System frequency for lumped BESS Topology A.

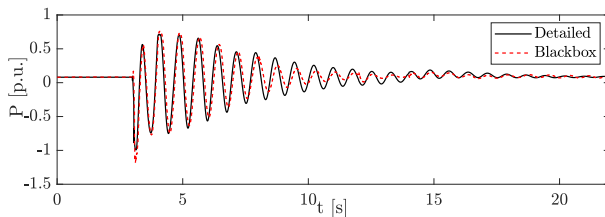


**Fig. 18.** Active power injections for Topology B.

generation outage in Topology A. In this case, the following four BESS models were compared.

- 1) *Complete*: It considers the VSC, dc-to-dc converter, battery bank, and their controls.
- 2) *Simplified*: It neglects the dc-to-dc converter and battery bank and models the VSC dc link as a constant source.
- 3) WECC: A widely used BESS model in academia and industry.
- 4) *Degraded*: Similar to the complete model but the batteries are assumed to be degraded, i.e., lower internal voltage and larger internal resistance are used.

Note that the BESS rapidly restores the frequency back to its nominal after the disturbance when providing SFC, while the frequency stabilizes at a different value with PFC only, which depends on the droop gain used in the frequency controller. Observe that when batteries are degraded, the frequency regulation performance is significantly affected because the BESS control system limits its active power injections. When the WECC model was used, the system frequency experienced a larger initial deviation.

Fast-acting ESSs, such as BESSs, can be used to damp low-frequency system oscillations by injecting active power in phase with the target undamped system frequency component; i.e.,  $-\Delta f_{\text{osc}}$ , due to oscillating generators. Thus, an ADN is connected to Bus 5 of the WSCC 9-bus benchmark system through a step-up transformer, in Topology B in Fig. 16. In the ADN, high penetration of PV generation is assumed, with ESS capacity spread across the distribution system, i.e., small units at households and larger units all aggregated at the MV level, corresponding to an equivalent 1.5-MVA PV and 1.5-MVA/2-MWh BESS at each of the 14 buses of the ADN, as shown in Fig. 16; simplified models for the loads and PV generation are used. A short circuit is applied at Bus 8 at  $t = 3$  s and then removed after 50 ms, while all BESSs are operating in the OD mode, for both the full ADN model and its aggregated model, while all the generator PSSs are disabled. In this case, it is shown in Fig. 18 that proper control of distributed BESSs can help to damp the low-frequency oscillations at the transmission level even in this small-scale BESS scenario and that the aggregated model based on NNs for  $P$  and  $Q$  injections of the ADN, i.e., NN-P and NN-Q, respectively, is able to properly represent the aggregated BESS response.

2) *Compressed Air Energy Storage*: In order to assess the benefits of ESSs adding physical inertia, a CAES system providing frequency regulation in the test system shown in Fig. 19, in which 30% of its demand is supplied by a wind farm, was studied in [30]. The performance of the CAES system was compared to an equivalent GT, with the former operating both in discharging mode and in simultaneous charging/discharging modes. Observe in Fig. 20 that the CAES system is more effective than the GT

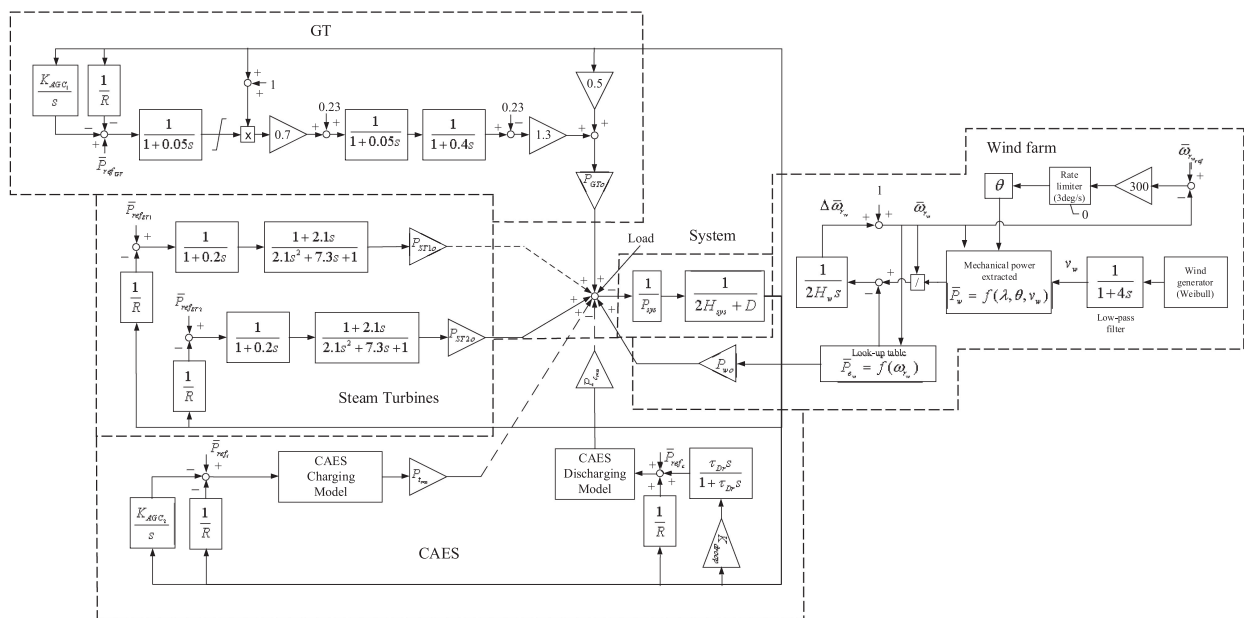


**Fig. 19.** System configuration for frequency regulation studies with CAES [30].

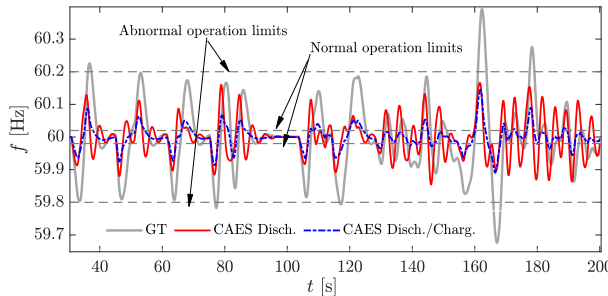


Fig. 20. Frequency regulation by CAES [30].

in regulating the system frequency, reducing the number of excursions beyond the allowed limits and the frequency deviations. Note also that the simultaneous charging and discharging modes yield the best results, further reducing the frequency deviations, mainly due to the inertia added by the compressor.

3) FESS: Another effective ESS technology for frequency regulation capability, simulations were performed for a 10-MVA FESS connected to a test system comprising a 10-MVA wind farm and 30-MVA TG supplying a 28.5-MW load, as shown in Fig. 21 [53]. Fig. 22 presents a comparison of system frequency when it is regulated by the FESS, with a base case when regulation is provided only by the traditional generating unit. Given the large size of the wind farm, the system frequency deviations are significant in the base case; however, when the FESS regulates the frequency, the deviations are practically eliminated.

4) ESSs in the Ontario Power System: Each component of the model in Fig. 15 was validated in [58] using the information provided by the IESO, which included a detailed dynamic model of the North American Eastern Interconnection and one year of data from the Ontario Power System and an FESS and BESS currently providing frequency regulation in Ontario. Since the data from two ESS facilities are included, the actual implementation of the model in Fig. 15 includes two sets of ESS blocks,

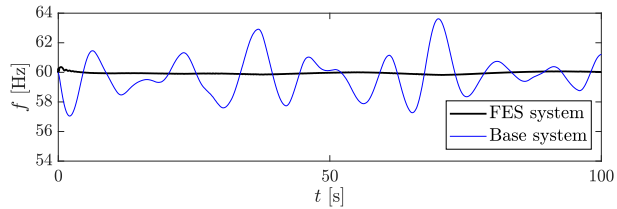


Fig. 22. Frequency regulation by FESS [53].

Stages V and VI, one pair for an FESS and the other for a BESS. A statistical comparison between the actual data and simulation results for the FESS and BESS is summarized in Table 2 for 6 of the 21 signals presented in Fig. 15, for one day (July 14, 2018) with 1-s resolution. Note that both the mean and standard deviations for each signal of the model are very similar, which implies that the model is capable of accurately replicating the behavior of actual components for the entire simulation period. Further detailed validation results for longer periods of time, up to one year, can be found in [58].

5) Microgrids: The Xeni Gwet'in First Nation community of Nemiah Valley in British Columbia, which is a battery-free PV-diesel off-grid network, was used as the test MG to investigate the feasibility of using TCLs such as EWHs, A/Cs, and GSHPs to help regulate the frequency of the MG [38]. The MG comprises a commercial complex and a residential zone with 22 houses, whose demand is supplied by two 95-kW diesel gensets operated one at the time and a 30-kW genset that operated during weeknights and weekends. In addition, PV generation is available in some of the houses, as shown in Fig. 23.

The MG frequency is defined based on the operating range of the 95-kW gensets, i.e., within 30% and 90% efficiency, which corresponds to frequency limits of  $f_{\max} = 61.37$  Hz and  $f_{\min} = 60.33$  Hz. Thus, a control logic that operates the EWH, A/C, and GSHP, available in all houses (except three), changes their temperature set points in proportion to the system frequency deviation such that they are turned on if the MG frequency is too high and turned off if the frequency is too low. This decentralized control architecture, which acts in addition to the genset's droop-based control, avoids the need for communication between the TCL and an MG's EMS, measuring the system frequency locally. The results of time-domain simulations for four cases considered are presented in Table 3 [38]. Comparing

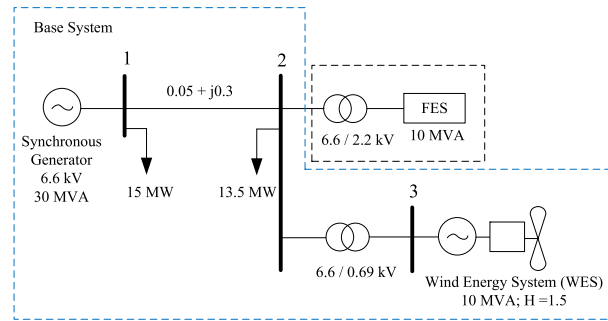
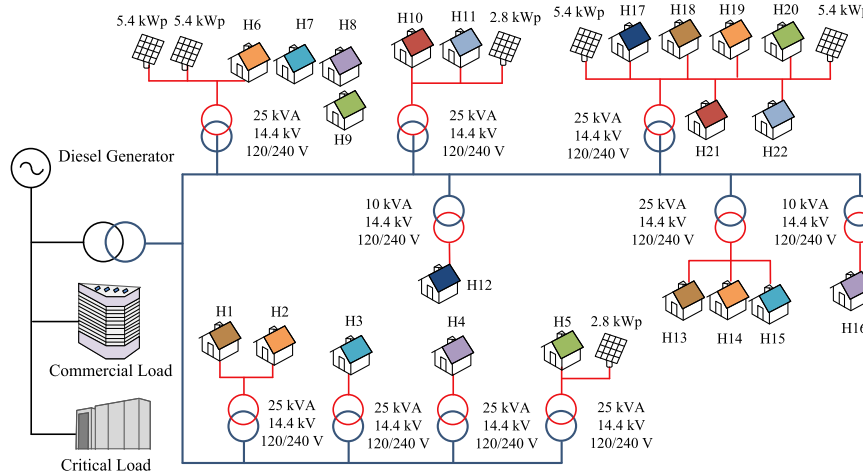


Fig. 21. Test system configuration [53].

Table 2 Validation of Frequency Regulation Model for Ontario (Fig. 15)

Stage and Output	Actual Data		Model Results	
	Mean [MW]	$\sigma$ [MW]	Mean [MW]	$\sigma$ [MW]
I ACE	32.61	80.79	32.01	80.86
II ACE <sub>filtered</sub>	19.85	79.6	19.96	81.64
III SR	-30.39	78.73	-35.88	80.68
IV P <sub>TGr</sub>	-30.40	75.73	-29.05	75.36
V SP <sub>FESS</sub>	-0.1277	0.5945	-0.129	0.5653
VI P <sub>FESS</sub>	-0.118	0.585	-0.120	0.565



**Fig. 23.** Nemiah Valley's test MG topology.

the length of time the system frequency exceeds limits in Case 1 (no TLC control) with the other cases, observe that TLC control can significantly improve the system frequency regulation, particularly when A/C (Case 3) and GSHP (Case 4) are used; the latter also presents the lowest fuel consumption and lowest frequency standard deviation  $\sigma$ .

## B. Peak Shaving

Peak shaving refers to the ability of large commercial and industrial customers to reduce their power consumption, particularly during peak hours when energy and demand charges are high. Some common ways in which customers can benefit from peak shaving include reducing their consumption, using local generation, or installing behind-the-meter ESSs, particularly for loads with limited flexibility.

In Ontario, as previously mentioned, electricity customers pay a monthly GAD charge, which covers the difference between the HOEP and the regulated rates for some nuclear and hydroelectric generating stations, the cost of building and maintaining new electricity infrastructure,

energy contracts, and delivering Ontario's conservation programs [57]. Large electricity customers, referred to as Class A, with an average peak demand above 5 MW, pay the GAD based on how much their peak demand use contributes to the top five provincial peaks during a base period (from May 1 to April 30). Hence, avoiding these five peak hours could significantly reduce their EnC. In fact, nowadays, this is the main electricity cost for Class A customers, outweighing the energy prices by a large margin [68]. The use of a behind-the-meter CAES system to reduce the load demand and energy drawn from the grid by an actual Ontario Class A customer with a peak demand of 14.27 MW was investigated in [60].

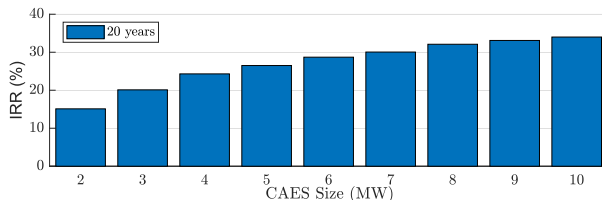
The customer has an existing cavern that can be repurposed for air storage, which reduces the capital cost. Thus, the optimal operation of the CAES system seeking to minimize the customer's total annual cost, i.e., EnC, GAD Cost GADC, and fixed and VOMC, was simulated assuming a fixed customer load and known HOEP and GAD values for that period. In Table 4, the energy savings for different CAES sizes, including no CAES, are summarized. Note that for CAES systems in the range of 2–10 MW, significant annual savings could be obtained; however, larger CAES sizes require larger initial investments. Hence, the IRR of different CAES system sizes in Table 4, considering initial investments in the range of 1500–3000 \$/kW and assuming the EnC savings as income, is presented in Fig. 24.

**Table 3** Frequency Regulation for Nemiah Valley's Test MG

		Cases			
TCL		1	2	3	4
Frequency	$f_{\max}$ [Hz]	61.98	61.57	61.62	61.57
	$f_{\min}$ [Hz]	59.83	60.20	60.33	60.35
	$\sigma$ [Hz]	0.447	0.255	0.251	0.244
Power	$P_{\max}$ [kW]	72.77	60.61	59.45	58.79
	$P_{\min}$ [kW]	11.61	25.50	25.01	23.97
Energy	EWHS [kWh]	174.8	175.3	177.6	178.8
	A/Cs [kWh]	28.91	28.7	27.88	-
	GSHPs [kWh]	-	-	-	18.06
Fuel consumption [l]		207	205	205.2	203.6
Time $f$ exceeds limits [%]		32.22	7.55	4.16	7.15

**Table 4** Customer's EnCs for Different CAES Sizes

CAES MW/MWh	GAC (\$)	EnG (\$)	OMC (\$)	TC (\$)	Savings (\$)
0	6,671,682	1,053,483	0	7,730,165	0
2/4	5,662,064	989,084	108,274	6,669,424	970,743
4/8	4,652,446	920,447	160,104	5,732,999	1,997,166
6/12	3,642,828	859,172	211,061	4,713,062	3,017,103
8/16	2,633,210	809,065	2060,387	3,702,663	4,027,501
10/20	1,623,592	769,301	308,353	2,701,246	5,028,919

**Fig. 24.** IRR for different CAES sizes.

Observe that if a typical MARR of 10% is considered, all investment options are reasonable, thus demonstrating that behind-the-meter storage, in particular CAES for the studied customer, would be an economically feasible solution to reduce EnCs.

### C. EA and Ancillary Services

Probably, the most common application for ESSs is EA, which entails charging when the price of energy is low and discharging when the price is high, thus achieving a revenue surplus operation from the price differential. This concept is not restricted to the energy market only since ESSs could also profit from participating in ancillary services or reserves markets as previously discussed. A notable feature that differentiates ESSs from typical generators is their S oC dependence, which constraints the time intervals when these systems can charge/discharge, thus adding a layer of complexity to their operation. In this case, the model to self-schedule the operation of an ESS acting as price taker must consider both the physical characteristics of the ESS as well as the main market uncertainties.

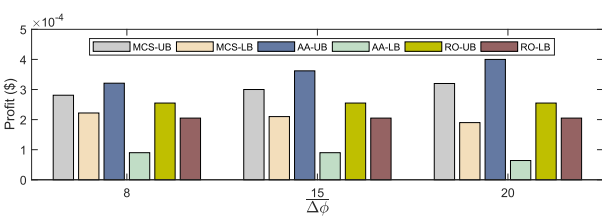
EA favors ESSs with large storage capacity. Currently, PH and CAES are the only two economically and technically feasible alternatives for bulk storage [16], [20], [69], with CAES being less restrictive in terms of its location, especially in North America, where abundant geological formations suitable to host underground caverns for air storage are available [70]. BESSs can also be used for arbitrage; however, they may need to provide additional grid services to become economically feasible [17]. For low-energy-density ESSs, such as FESS, arbitrage is less attractive, particularly due to its relatively large self-discharge losses [21]. On the other hand, the fast response, high ramp rates, and capability to provide upward and downward response of most ESSs (e.g., CAES, BESS, and FESS) make these technologies more suitable for ancillary services such as frequency regulation reserves. TESSs are mostly used to help optimally supply the local energy needs of buildings (residential, commercial, or industrial); therefore, their most common applications are load leveling and peak shaving, through DR. EAs are less common grid services for TESS; however, these systems may also be used for frequency regulation reserves, as shown in Section IV-A5 and discussed, for example, in [23].

1) *Compressed Air Energy Storage* : As an arbitrage and ancillary services application, a 100-MW charging/60-MW

discharging CAES participating in Ontario's energy, SR, and idle reserve markets was studied in [39] and [61]. This facility has a minimum discharging and charging rates of 30 and 25 MW, respectively, a quick start capacity of 40 MW, and it seeks to maximize its profit for volatile prices. Accordingly, the CAES would discharge or offer its reserve capacity when prices in the respective markets are high or charge when the prices are low. As highlighted in Section III-G, price uncertainties can be handled using RO, AA, or MCSs; thus, these three approaches were used to obtain the optimal CAES schedule that maximizes its daily profits. The RO simulations considered a risk-profit tradeoff based on combinations of price variations  $\overline{\Delta\phi} \in [8\%, 15\%, 20\%]$  and uncertainty budget  $\Gamma \in [0, 5, 10, 15, 20, 24]$ , with larger  $\Gamma$  values yielding higher  $\overline{\Delta\phi}$  values providing more financial protection against large price mismatches, both resulting in lower profits. The AA approach, on the other hand, yields a single optimum schedule interval based on the  $\overline{\Delta\phi}$  value; thus, large  $\overline{\Delta\phi}$  values produce large profit radius and center values and, hence, larger profit intervals. MCS based on several random prices and uniform probability density functions (pdfs), with the prices varying within the same range  $\overline{\Delta\phi}$ , was used for validation purposes.

The CAES's profit upper bounds (UBs) and lower bounds (LBs) obtained using RO, AA, and MC for different values of  $\overline{\Delta\phi}$  are shown in Fig. 25. Note that as  $\overline{\Delta\phi}$  increases, so do the intervals, which is reasonable, given the wider range of prices. In RO, the UP and LB correspond to  $\Gamma = 0$  (deterministic case) and  $\Gamma = 24$  (most conservative case), respectively, while the bounds in the AA case depend directly on  $\overline{\Delta\phi}$ . Observe that AA yields the largest intervals for all  $\overline{\Delta\phi}$ . Since MCS presents a much larger computational burden than AA or RO, the latter would be preferred to solve the optimal schedule of the plant on a daily basis.

2) *GSHP Aggregation*: The aggregation of residential demand for the participation on a DA and RT electricity markets was studied in [39], [61] for Ontario, using GSHP as an alternative to conventional HVAC systems. In the DA market, the aggregator forecasts the electricity market price, and ambient temperature for the next day, and along with information of the uncontrolled loads of the aggregated houses, optimally schedules their individual

**Fig. 25.** Profits for a CAES price-taker facility for MCS, AA, and RO methodologies.

**Table 5** Aggregator Results With HVAC and GSHP Systems

		Cost (\$)		Heating Energy (kWh)	
		HVAC	GSP	HVAC	GSP
Max Comfort		5,700	4,999	68,645	53,655
Min. Cost	DA	4,499	4,576	61,229	52,096
	RT	133	68	65,625	52,096
Total		5,078	4,645		

thermal loads such that their total electricity cost is minimized while satisfying the houses' temperature comfort range. These schedules can be used by the aggregator to submit hourly energy bids to the wholesale market for the next day. For the RT market, the temperature and uncontrolled loads forecasts are updated, and the thermal loads are dispatched in RT to minimize the aggregator's total penalty payable for deviations from the DA dispatch, at a market price that is not affected by the aggregator's decision.

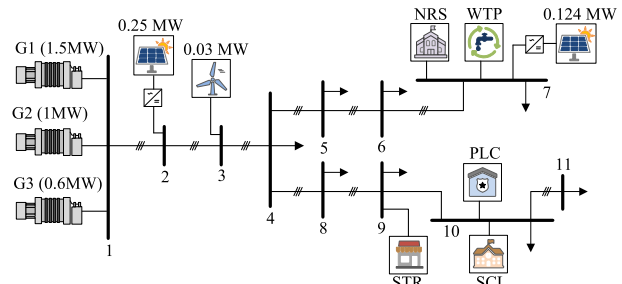
In Table 5, the results for the aggregation of 800 houses located in Ontario, on a cold winter day, are presented for cases in which the aggregator maximizes the customers' comfort or minimizes the households' total electricity costs [39]. This study assumed that people leave their houses at 08:00 and return at 18:00; the house thermostat set points are kept constant at 22 °C during this period to maximize comfort, while these set points are relaxed when minimizing cost. The study also compared the aggregation when heat is supplied by conventional HVAC units and GSHPs in the houses. Note that the aggregator's total costs and energy consumed based on GSHPs are lower than with HVAC, thus demonstrating that the former would be preferable for space heating.

#### D. Microgrid EMS

ESSs play a central role in enabling the operation of MGs in stand-alone mode, particularly when relying on intermittent renewable generation such as PV or wind. In fossil fuel-based MGs, ESSs can help to decrease fuel consumption by allowing the existing generation to operate at their most efficient operating points, reducing the required installed generation capacity, including backup generation. Furthermore, MGs can also benefit from TESS to more efficiently supply their thermal demand, including space and WH.

1) *Kasabonika Lake First Nation*: This is an isolated community located in Northern Ontario, Canada. Its MG comprises three 10-kW and one 30-kW wind turbines, three gensets of 1.5 MW, 1 MW, and 0.6 MW, operated one at a time, and 12.4-MW roof-top PV generation, with a 250-kW PV plant planned at some point. The total peak demand is approximately 850 kW, which corresponds to residential and commercial loads, including a store (STR), school (SCL), police station (PLS), nursery station (NRS), and a water treatment plant (WTP), as shown in Fig. 26 [37].

A study was carried out to determine the possible use of TESS to supply part of KLFN's estimated heating demand,

**Fig. 26. KLFN MG.**

which is approximately 30% of the total residential electrical demand. Hence, three cases were considered: 1) no TESS; 2) 50%; and 3) 100% of the heating demand being replaced by a brick-core TESS. The total operating cost, net peak demand, and gensets' on time for six days of operation of the KLFN MG are summarized in Table 6. The results demonstrate that when TESS is available, operating the MG is cheaper, particularly when PV is available, with around 30% cost reduction for a 100% of TESS supplying the thermal demand. Also, generators operate at higher efficiencies, resulting in G3 being dispatched for longer periods, whereas the MG demand is not high enough for G1 to be dispatched.

2) *Innovative Process of Energy Conversion (PrInCE)*: This MG, shown in Fig. 13, is a facility built at the Electric Power System Laboratory, Politecnico di Bari, Bari, Italy [36]. It supplies the electricity and heat needs of a warehouse hosting offices and laboratories and is characterized by strong coupling between its thermal and electrical subsystems. The three-phase low-voltage network contains a 50-kW PV plant, a 60-kVA wind turbine emulator, a 70-kVA BESS, a 120-kVA natural-gas fuelled reciprocating engine unit (CHP1), and a 30-kVA gas microturbine (CHP2) supplying two 150-kVA programmable loads. In addition, the heat demand of the building is supplied by a heat pump consuming power from the MG and two boilers that heat up a water tank acting as TESS, which is also fed by the remnant heat from two generating units. Thus, an EMS that integrates the electrical and thermal subsystems was developed and simulated, seeking to minimize the MG's operational cost by coordinating all controllable assets to satisfy the electrical and thermal demands for two winter days, with Day 2 being colder than Day 1. The results showed that the EMS could significantly reduce the overall

**Table 6** KLFN MG Dispatch for Different TESS Penetration Levels

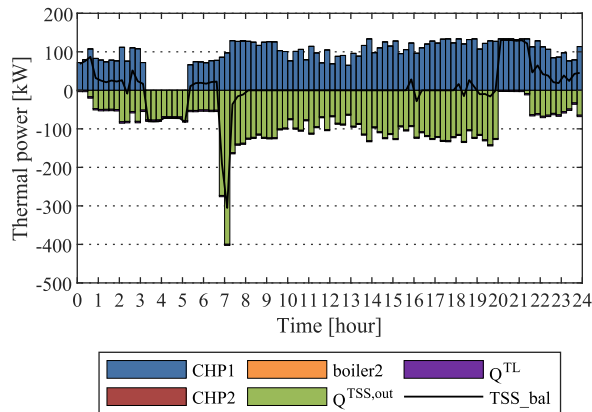
250 kW PV	Case	Operating Cost of MG [\$]	Peak Demand [kW]	Total ON Time [t]		
				G1	G2	G3
No	I	45,724	771	-	97	47
	II	43,574	734	-	89	55
	III	40,220	790	-	73	71
Yes	I	42,632	771	-	90	54
	II	36,710	725	-	65	79
	III	32,898	772	-	49	95

**Table 7** PrInCE MG Dispatch Summary for Two Winter Days

Daily Costs for the EMS						
Day	Opt. total cost [€]	Total elect. consump. [kWh]	Average elect. cost [€/kWh]	CHP units [€]	Boilers [€]	Net heat demand [kWh]
1	300.52	1,879.17	0.1588	298.39	2.13	2,225.44
2	348.41	1,824.51	0.1774	323.75	24.66	3,090.64

Daily Costs for the Electrical-Only EMS						
Day	Opt. elect. cost [€]	Total elect. consump. [kWh]	Average elect. cost [€/kWh]	Cost of heat supply [€]	Total cost [€]	Cost incr. [%]
1	424.58	281.21	1,770.43	0.1588	143.37	+41.3
2	496.46	297.35	1,650.60	0.1801	199.11	+42.5

**Fig. 27.** PrInCE MG TESS power balance [36].

energy supply costs for both days, compared to a case when no coordination between thermal and electrical systems is considered, as summarized in Table 7.

Since the EMS aims to minimize the EnC, the temperature in the building mostly followed the lower band of the building's thermostat set points so that the HP is used less, and less heat is extracted from the TESS. The BESS mostly charges from the excess of renewable resources in the morning and discharges when these yield limited power in the evening. On the other hand, the TESS discharges as

the temperature difference between the ambient conditions and the building varies through the day or the thermostat set points change. Fig. 27 shows the thermal power balance in the MG, with the blue bars representing the heat power provided by CHP 1, the green bars representing the discharging power of the TESS, and the black line representing the TESS balance, where positive values represent the TESS charge and negative values corresponding to its discharge.

## V. CONCLUSION

In this article, novel models for dynamic electrical grid studies and market integration of BESS, FESS, CAES, and TESS were discussed. The main features, topologies, power conditioning system, and control strategies of each ESS were described, and state-of-the-art models of ESS for dynamic operation, planning, and market integration studies were presented. Finally, ESS applications in actual grids or benchmarks were investigated focusing on BESS, CAES, FESS, and TESS providing frequency and voltage regulation, OD, peak shaving, and EA and ancillary services in power grids and MGs, demonstrating the benefits of ESS for grid performance and economics.

Future research should explore how different ESS technologies can be coordinated to further improve the services they can provide, either as stand-alone hybrid energy storage facilities (e.g., batteries with thermal storage) or distributed (e.g., home BESS and EVs) in an electrical grid, taking advantage of their specific characteristics. Furthermore, the need to study and apply ESS as grid-forming generators to enable 100% RES bulk power systems, based on similar and proven MG applications, is rapidly evolving as a fundamental part of net-zero energy systems. All this will require extensive work toward the effective integration of different modeling domains, as well as new improved interfaces and control strategies. Furthermore, as more sensing data become available in bulk power grids and MGs, data-driven modeling based on artificial intelligence should be investigated as realistic alternatives to the existing traditional modeling techniques for ESS, as demonstrated for BESS in this review. ■

## REFERENCES

- X. Liu, M. Shahidehpour, Z. Li, X. Liu, Y. Cao, and Z. Bie, "Microgrids for enhancing the power grid resilience in extreme conditions," *IEEE Trans. Smart Grid*, vol. 8, no. 2, pp. 589–597, Mar. 2017.
- R. H. A. Zubro and G. Mokryani, "Active distribution network operation: A market-based approach," *IEEE Syst. J.*, vol. 14, no. 1, pp. 1405–1416, Mar. 2020.
- G. Chaspierre, G. Denis, P. Panciatici, and T. Van Cutsem, "A dynamic equivalent of active distribution network: Derivation, update, validation and use cases," *IEEE Open Access J. Power Energy*, vol. 8, pp. 497–509, 2021.
- T. Morstyn, B. Hredzak, and V. G. Agelidis, "Control strategies for microgrids with distributed energy storage systems: An overview," *IEEE Trans. Smart Grid*, vol. 9, no. 4, pp. 3652–3666, Jul. 2018.
- E. Hossain, J. Hossain, and F. Un-Noor, "Utility grid: Present challenges and their potential solutions," *IEEE Access*, vol. 6, pp. 60294–60317, 2018.
- R. H. Byrne, T. A. Nguyen, D. A. Copp, B. R. Chalamala, and I. Gyuk, "Energy management and optimization methods for grid energy storage systems," *IEEE Access*, vol. 6, pp. 13231–13260, 2017.
- S. O. Showers and A. K. Raji, "Benefits and challenges of energy storage technologies in high penetration renewable energy power systems," in *Proc. IEEE PES/IAS PowerAfrica*, Abuja, Nigeria, Aug. 2019, pp. 209–214.
- M. Hayes and S. Hoff, "Large battery systems are often paired with renewable energy power plants," U.S. Energy Inf. Admin., Washington, DC, USA, Tech. Rep., May 2020. [Online]. Available: <https://www.eia.gov/todayinenergy/detail.php?id=43775>
- W. Gorman, C. C. Montañés, A. Mills, J. H. Kim, D. Millstein, and R. Wiser, "Are coupled renewable-battery power plants more valuable than independently sited installations?" *Energy Econ.*, vol. 107, pp. 1–48, Mar. 2022.
- U. Datta, A. Kalam, and J. Shi, "Battery energy storage system to stabilize transient voltage and frequency and enhance power export capability," *IEEE Trans. Power Syst.*, vol. 34, no. 3, pp. 1845–1857, May 2019.
- M. Farrokhabadi *et al.*, "Microgrid stability definitions, analysis, and examples," *IEEE Trans. Power Syst.*, vol. 35, no. 1, pp. 13–29, Jan. 2020.
- X. Li, Z. Li, L. Guo, J. Zhu, Y. Wang, and C. Wang, "Enhanced dynamic stability control for low-inertia hybrid AC/DC microgrid with distributed energy storage systems," *IEEE Access*, vol. 7, pp. 91234–91242, 2019.
- M. Farhad and O. Mohammed, "Energy storage technologies for high-power applications," *IEEE Trans. Ind. Appl.*, vol. 52, no. 3, pp. 1953–1961, May/Jun. 2016.
- A. Ortega and F. Milano, "Modeling, simulation, and comparison of control techniques for energy storage systems," *IEEE Trans. Power Syst.*, vol. 32, no. 3, pp. 2445–2454, May 2017.
- X. Luo, J. Wang, M. Dooner, and J. Clarke,

- "Overview of current development in electrical energy storage technologies and the application potential in power system operation," *Appl. Energy*, vol. 137, pp. 511–536, Jan. 2015.
- [16] V. A. Boicea, "Energy storage technologies: The past and the present," *Proc. IEEE*, vol. 102, no. 11, pp. 1777–1794, Nov. 2014.
- [17] "IESO report: Energy storage," *Independ. Electr. Syst. Operator*, Toronto, ON, Canada, Tech. Rep., Mar. 2016. [Online]. Available: [http://www.ieso.ca/-/media/files/ieso/documents/library/energy-storage/ieso-energy-storage-report\\_march\\_2016.pdf](http://www.ieso.ca/-/media/files/ieso/documents/library/energy-storage/ieso-energy-storage-report_march_2016.pdf)
- [18] M. C. Lott and S.-I. Kim, "Technology roadmap—Energy storage," Int. Energy Agency, Paris, France, Tech. Rep., Mar. 2014. [Online]. Available: [https://iea.blob.core.windows.net/assets/80b629ee-597b-4f79-a236-3b9a36aede/Technology\\_RoadmapEnergystorage.pdf](https://iea.blob.core.windows.net/assets/80b629ee-597b-4f79-a236-3b9a36aede/Technology_RoadmapEnergystorage.pdf)
- [19] A. A. Akhil et al., "DOE/EPRI 2013 electricity storage handbook in collaboration with NRECA," Sandia Nat. Laboratories, Albuquerque, NM, USA, Tech. Rep. SAND2013-5131, Jul. 2013. [Online]. Available: <https://www.energy.gov/sites/default/files/2013/08/f2/ElecStorageIndbk2013.pdf>
- [20] P. Nikolaidis and A. Poullikkas, "A comparative review of electrical energy storage systems for better sustainability," *J. Power Technol.*, vol. 97, no. 3, pp. 220–245, 2017.
- [21] M. E. Amiryar and K. R. Pullen, "A review of flywheel energy storage system technologies and their applications," *Appl. Sci.*, vol. 7, no. 3, pp. 1–21, Mar. 2017.
- [22] S. Vazquez, S. M. Lukic, E. Galvan, L. G. Franquelo, and J. M. Carrasco, "Energy storage systems for transport and grid applications," *IEEE Trans. Ind. Electron.*, vol. 57, no. 12, pp. 3881–3895, Dec. 2010.
- [23] D. Enescu, G. Chicco, R. Porumb, and G. Seritan, "Thermal energy storage for grid applications: Current status and emerging trends," *Energies*, vol. 13, no. 2, pp. 1–21, 2020.
- [24] S. Koohi-Fayegh and M. A. Rosen, "A review of energy storage types, applications and recent developments," *J. Energy Storage*, vol. 27, pp. 1–23, Feb. 2020.
- [25] "Energy storage grand challenge: Energy storage market report," U.S. Dept. Energy, Washington, DC, USA, Tech. Rep., NREL/TP-5400-78461 DOE/GO-102020-5497, Dec. 2020.
- [26] W. Kramer, S. Chakraborty, B. Kroposki, and H. Thomas, "Advanced power electronic interfaces for distributed energy systems part 1: Systems and topologies," *Nat. Renew. Energy Lab. (NREL)*, Golden, CO, USA, Tech. Rep., NREL/TP-581-42672, Mar. 2008.
- [27] M. Ghanaaian and S. Loftifard, "Control of flywheel energy storage systems in the presence of uncertainties," *IEEE Trans. Sustain. Energy*, vol. 10, no. 1, pp. 36–45, Jan. 2019.
- [28] "NRStor Project Spotlight: 2MW/500kWh Minto Flywheel Project," Brochure, NRStor, Toronto, ON, Canada, 2022. [Online]. Available: <http://nrstor.com/wp-content/uploads/2019/06/flywheels.pdf>
- [29] "Operating Plants," Beacon Power, Tyngsborough, MA, USA, 2022. [Online]. Available: <https://beaconpower.com/stephentown-new-york/>
- [30] I. Calero, C. A. Canizares, and K. Bhattacharya, "Compressed air energy storage system modeling for power system studies," *IEEE Trans. Power Syst.*, vol. 34, no. 5, pp. 3359–3371, Sep. 2019.
- [31] S. Succar and R. H. Williams, "Compressed air energy storage: Theory, resources, and applications for wind power," Princeton Environ. Inst., Princeton, NJ, USA, Tech. Rep., 2008. [Online]. Available: [https://acee.princeton.edu/wp-content/uploads/2016/10/SuccarWilliams\\_PEI\\_CAES\\_2008April8.pdf](https://acee.princeton.edu/wp-content/uploads/2016/10/SuccarWilliams_PEI_CAES_2008April8.pdf)
- [32] "Huntorf air storage gas turbine power plant," Brown, Boveri & Cie, Baden, Switzerland, Tech. Rep., DGK90202E, 1979.
- [33] R. Carnegie, D. Gotham, D. Nderitu, and P. V. Preckel, "Utility scale energy storage systems, benefits, application, and technologies," State Utility Forecasting Group, West Lafayette, IN, USA, Tech. Rep., Jun. 2013.
- [34] R. B. Schainker and M. Nakhamkin, "Compressed-air energy storage (CAES): Overview, performance and cost data for 25 MW to 220 MW plants," *IEEE Trans. Power App. Syst.*, vol. PAS-104, no. 4, pp. 790–795, Jul. 1985.
- [35] "Goderich A-CAES facility," Hydrostor, Toronto, ON, Canada, Tech. Rep., 2021. [Online]. Available: <https://www.hydrostor.ca/goderich-a-caes-facility/>
- [36] W. Violante, C. A. Canizares, M. A. Trovato, and G. Forte, "An energy management system for isolated microgrids with thermal energy resources," *IEEE Trans. Smart Grid*, vol. 11, no. 4, pp. 2880–2891, Jul. 2020.
- [37] P. S. Sauter, B. V. Solanki, C. A. Canizares, K. Bhattacharya, and S. Hohmann, "Electric thermal storage system impact on northern communities' microgrids," *IEEE Trans. Smart Grid*, vol. 10, no. 1, pp. 852–863, Jan. 2019.
- [38] W. Mendieta and C. A. Canizares, "Primary frequency control in isolated microgrids using thermostatically controllable loads," *IEEE Trans. Smart Grid*, vol. 12, no. 1, pp. 93–105, Jan. 2021.
- [39] D. Peralta, K. Bhattacharya, and C. Canizares, "Ground source heat pump modeling and aggregation for services provision in electricity markets," in *Proc. IEEE Power Energy Soc. Gen. Meeting (PESGM)*, Montreal, QC, Canada, Aug. 2020, pp. 1–5.
- [40] M. Farrokhbadi, S. König, C. A. Cañizares, K. Bhattacharya, and T. Leibfried, "Battery energy storage system models for microgrid stability analysis and dynamic simulation," *IEEE Trans. Power Syst.*, vol. 33, no. 2, pp. 2301–2312, Mar. 2018.
- [41] F. Calero, C. A. Canizares, and K. Bhattacharya, "Dynamic modeling of battery energy storage and applications in transmission systems," *IEEE Trans. Smart Grid*, vol. 12, no. 1, pp. 589–598, Jan. 2021.
- [42] M. Chen and G. A. Rincon-Mora, "Accurate electrical battery model capable of predicting runtime and  $I-V$  performance," *IEEE Trans. Energy Convers.*, vol. 21, no. 2, pp. 504–511, Jun. 2006.
- [43] D. Bazargan, S. Filizadeh, and A. M. Gole, "Stability analysis of converter-connected battery energy storage systems in the grid," *IEEE Trans. Sustain. Energy*, vol. 5, no. 4, pp. 1204–1212, Oct. 2014.
- [44] "Wind Energy R&D Park and Storage System for Innovation in Grid Integration," Wind Energy Inst. Canada (WEICAN), Tignish, PE, Canada, 2020. [Online]. Available: <https://www.nrcan.gc.ca/science-and-data/funding-partnerships/funding-opportunities/current-investments/wind-energy-rd-park-and-storage-system-innovation-grid-integration/4979>
- [45] I. Calero, C. A. Canizares, and K. Bhattacharya, "Implementation of transient stability model of compressed air energy storage systems," *IEEE Trans. Power Syst.*, vol. 35, no. 6, pp. 4734–4744, Nov. 2020.
- [46] P. Kundur, N. Balu, and M. Lauby, *Power System Stability and Control*. New York, NY, USA: McGraw-Hill, 1994.
- [47] A. Gomez-Exposito, A. J. Conejo, and C. Canizares, *Electric Energy Systems: Analysis and Operation*. Boca Raton, FL, USA: CRC Press, 2016.
- [48] Y. Cengel and M. Boles, *Thermodynamics: An Engineering Approach*, 8th ed. New York, NY, USA: McGraw-Hill, 2002.
- [49] T. Schütz, H. Harb, R. Strelbow, and D. Müller, "Comparison of models for thermal energy storage units and heat pumps in mixed integer linear programming," in *Proc. 28th Int. Conf. ECOS*, Pau, France, Jul. 2015, pp. 1–12.
- [50] F. Calero, "Impact of distributed battery energy storage on electric power transmission and distribution systems," Ph.D. dissertation, Dept. Elect. Comput. Eng., Univ. Waterloo, Waterloo, ON, USA, 2021.
- [51] "WECC battery storage dynamic modeling guideline," Modeling and Validation Work Group, WECC, Salt Lake City, UT, USA, Tech. Rep., 2016.
- [52] P. Pourbeik, "Proposal for new features for the renewable energy system generic models," WECC, Salt Lake City, UT, USA, Tech. Rep., 2019.
- [53] D. Peralta, C. Canizares, and K. Bhattacharya, "Practical modeling of flywheel energy storage for primary frequency control in power grids," in *Proc. IEEE Power Energy Soc. Gen. Meeting (PESGM)*, Portland, OR, USA, Aug. 2018, pp. 1–5.
- [54] G. O. Cimua, C. Saudemont, B. Robyns, and M. M. Radulescu, "Control and performance evaluation of a flywheel energy-storage system associated to a variable-speed wind generator," *IEEE Trans. Ind. Electron.*, vol. 53, no. 4, pp. 1074–1085, Jun. 2006.
- [55] G. Cimua, S. Breban, M. M. Radulescu, C. Saudemont, and B. Robyns, "Design and control strategies of an induction-machine-based flywheel energy storage system associated to a variable-speed wind generator," *IEEE Trans. Energy Convers.*, vol. 25, no. 2, pp. 526–534, Jun. 2010.
- [56] F. Calero, C. A. Canizares, and K. Bhattacharya, "Aggregated BESS dynamic models for active distribution network studies," *IEEE Trans. Smart Grid*, vol. 12, no. 3, pp. 2077–2088, May 2021.
- [57] "Independent Electricity System Operator (IESO): Connecting Today. Powering Tomorrow," *Independ. Electr. Syst. Operator*, Toronto, ON, USA, 2021. [Online]. Available: <http://www.ieso.ca/>
- [58] N. S. Guzman, C. A. Canizares, K. Bhattacharya, and D. Sohm, "Frequency regulation model of bulk power systems with energy storage," *IEEE Trans. Power Syst.*, vol. 37, no. 2, pp. 913–926, Mar. 2022.
- [59] E. N. S. Guzman, M. Arriaga, C. A. Canizares, J. W. Simpson-Porco, D. Sohm, and K. Bhattacharya, "Regulation signal design and fast frequency control with energy storage systems," *IEEE Trans. Power Syst.*, vol. 37, no. 1, pp. 224–236, Jan. 2022.
- [60] C. C. Anierobi, K. Bhattacharya, and C. A. Canizares, "Behind-the-meter compressed air energy storage feasibility and applications," *Electr. Power Syst. Res.*, vol. 189, pp. 1–7, Dec. 2020.
- [61] D. Peralta, K. Bhattacharya, and C. Canizares, "Ground source heat pump modeling, operation, and participation in electricity markets," *IEEE Trans. Smart Grid*, vol. 13, no. 2, pp. 1126–1138, Mar. 2022.
- [62] N. Padmanabhan, M. Ahmed, and K. Bhattacharya, "Battery energy storage systems in energy and reserve markets," *IEEE Trans. Power Syst.*, vol. 35, no. 1, pp. 215–226, Jan. 2020.
- [63] "Electric storage participation in markets operated by regional transmission organizations and independent system operators, order no. 841," Federal Energy Regulatory Commission (FERC), Washington, DC, USA, Tech. Rep., Feb. 2018. [Online]. Available: <https://ferc.gov/sites/default/files/2020-06/Order-841.pdf>
- [64] "Frequency regulation compensation in the organized wholesale power markets, order no. 755," Federal Energy Regulatory Commission (FERC), Washington, DC, USA, Tech. Rep., Oct. 2011. [Online]. Available: <https://www.ferc.gov/sites/default/files/2020-06/OrderNo.755.pdf>
- [65] B. Xu, Y. Dvorkin, D. S. Kirschen, C. A. Silva-Monroy, and J.-P. Watson, "A comparison of policies on the participation of storage in U.S. frequency regulation markets," in *Proc. IEEE Power Energy Soc. Gen. Meeting (PESGM)*, Boston, MA, USA, Jul. 2016, pp. 1–5.
- [66] M. F. Z. de Souza, C. A. Canizares, and K. Bhattacharya, "Self-scheduling models of a CAES facility under uncertainties," *IEEE Trans. Power Syst.*, vol. 36, no. 4, pp. 3607–3617, Jul. 2021.
- [67] F. Calero, C. A. Canizares, and K. Bhattacharya, "Detailed and average battery energy storage model comparison," in *Proc. IEEE PES Innov. Smart Grid Technol. Eur. (ISGT-Europe)*, Bucharest, Romania, Sep. 2019, pp. 1–5.
- [68] "Regulated price plan, price report," Ontario Energy Board, Toronto, ON, Canada, Tech. Rep., Apr. 2021.
- [69] B. Cleary, A. Duffy, A. O'Connor, M. Conlon, and V. Fthenakis, "Assessing the economic benefits of compressed air energy storage for mitigating wind curtailment," *IEEE Trans. Sustain. Energy*, vol. 6, no. 3, pp. 1021–1028, Jul. 2015.
- [70] L. D. Mears and H. L. Gotschall, "EPRI-DOE handbook of energy storage for transmission & distribution applications," EPRI and U.S. Dept. Energy, Palo Alto, CA, USA, Tech. Rep., 2003.

**ABOUT THE AUTHORS**

**Fabian Calero** (Member, IEEE) received the Diploma degree in electrical engineering from the Escuela Politécnica Nacional (EPN), Quito, Ecuador, in 2007, and the Ph.D. degree in electrical and computer engineering from the University of Waterloo, Waterloo, ON, Canada, in 2020.

His research interests include power system modeling and control, and artificial intelligence applications for dynamic modeling.



**Claudio A. Cañizares** (Fellow, IEEE) has been a University Professor and the Hydro One Endowed Chair with the Department of Electrical and Computer Engineering, University of Waterloo, Waterloo, ON, Canada, since 1993. His highly cited research focuses on modeling, simulation, computation, stability, control, and optimization of power and energy systems.

Prof. Cañizares is a Fellow of the Royal Society of Canada and the Canadian Academy of Engineering. He was a recipient of the 2017 IEEE PES Outstanding Power Engineering Educator Award, the 2016 IEEE Canada Electric Power Medal, and multiple awards and recognitions from PES Technical Committees. He is also the Editor-in-Chief of IEEE TRANSACTIONS ON SMART GRID.



**Kankar Bhattacharya** (Fellow, IEEE) received the Ph.D. degree in electrical engineering from IIT Delhi, New Delhi, India, in 1993.

He was with the Faculty of Indira Gandhi Institute of Development Research, Mumbai, India, from 1993 to 1998, and the Department of Electric Power Engineering, Chalmers University of Technology, Gothenburg, Sweden, from 1998 to 2002. In 2003, he joined the Department of Electrical and Computer Engineering, University of Waterloo, Waterloo, ON, Canada, where he is currently a Full Professor. His current research interests include power system economics and operational aspects.

Dr. Bhattacharya is a Registered Professional Engineer in the Province of Ontario.



**Chioma Anierobi** (Member, IEEE) received the B.Sc. and M.Eng. degrees in electrical engineering from Nnamdi Azikiwe University, Awka, Nigeria, in 2009 and 2015, respectively, and the M.Sc. degree in electrical and computer engineering from the University of Waterloo, Waterloo, ON, Canada.

She was a Lecturer with the Department of Electrical Engineering, Nnamdi Azikiwe University, from 2012 to 2016. She is currently a Power Consultant at CPCS Transcom Ltd., Ottawa, ON, Canada. Her research interests include energy storage systems, power system optimization, and renewable energy investments in developing countries.



**Ivan Calero** (Member, IEEE) received the Diploma degree in electrical engineering from the Escuela Politécnica Nacional (EPN), Quito, Ecuador, in 2008, and the Ph.D. degree in electrical and computer engineering from the University of Waterloo, Waterloo, ON, Canada, in 2020.

From 2009 to 2010, he was with the National Electricity Council of Ecuador, Quito. He is currently a Postdoctoral Fellow with the University of Waterloo. His research interests include modeling, analysis, and control of power systems.



**Matheus F. Zambroni de Souza** (Student Member, IEEE) received the Diploma and master's degrees in electrical engineering from the Universidade Federal de Itajubá (UNIFEI), Itajubá, Brazil, in 2015 and 2017, respectively. He is currently working toward the Ph.D. degree in electrical engineering at the University of Waterloo, Waterloo, ON, Canada.



He had experience working with power systems stability during his Diploma degree and power quality and signal processing during his master's degree. Today, his research focuses on compressed air energy storage participation in the electricity market, using robust optimization and/or affine arithmetic to model uncertainties.

**Mostafa Farrokhabadi** (Member, IEEE) received the B.Sc. degree in electrical engineering from the Amirkabir University of Technology, Tehran, Iran, in 2010, the M.Sc. degree in electric power engineering from the KTH Royal Institute of Technology, Stockholm, Sweden, in 2012, and the Ph.D. degree in electrical and computer engineering from the University of Waterloo, Waterloo, ON, Canada, in 2017.



He was a Postdoctoral Fellow with the University of Waterloo from 2017 to 2018. He is currently the Vice President of Bluwave-ai, Inc., Ottawa, ON, Canada. His research interests include modeling, control, and optimization in microgrids.

**Noela Sofia Guzman** (Student Member, IEEE) received the B.Sc. degree (*summa cum laude*) in electrical engineering from the Escuela Politécnica Nacional (EPN), Quito, Ecuador, in 2014, and the Ph.D. degree from the Department of Electrical and Computer Engineering, University of Waterloo, Waterloo, ON, Canada, in 2021.



From 2014 to 2016, she worked as a Technical Assistant at the Electricity Corporation of Ecuador—Business Unit Transelectric, Quito. Her current research interests include power systems, modeling, optimization, frequency regulation, and energy storage systems.

**William Mendieta** (Student Member, IEEE) received the Diploma degree in electrical engineering from the University of Cuenca, Cuenca, Ecuador, in 2013, and the M.A.Sc. degree in electrical and computer engineering from the University of Waterloo, Waterloo, ON, Canada, in 2019. He is currently working toward the Ph.D. degree at the School of Electrical and Electronic Engineering, University College Dublin, Dublin, Ireland.



He has previously worked as a protection and control engineer for generation, transmission, and distribution system networks. His research interests include modeling, analysis, and control of power systems.

**Dario Peralta** (Student Member, IEEE) graduated in electrical engineering (specialization in electric transmission protections) from the Escuela Superior Politécnica del Litoral (ESPOL), Guayaquil, Ecuador, in 2009. He received the M.A.Sc. degree in electrical engineering from the University of Waterloo, Waterloo, ON, Canada, in 2017, where he is currently working toward the Ph.D. degree.



His research interests include energy storage system modeling and application to power grids and electricity markets.

**Bharatkumar V. Solanki** (Member, IEEE) received the bachelor's degree in electrical engineering from Gujarat University, Ahmedabad, India, in 2009, the master's degree in electrical engineering from the Maharaja Sayajirao University of Baroda, Vadodara, India, in 2011, and the Ph.D. degree in electrical and computer engineering from the University of Waterloo, Waterloo, ON, Canada, in April 2018.



He worked as an Analog Hardware Design Engineer at ABB Global Industries and Service Ltd., Vadodara, from 2011 to 2013. He is currently a Technical Lead for microgrid projects, Siemens Canada, Mississauga, ON, Canada. His research interests include modeling, simulation, control, and optimization of power systems.

**Nitin Padmanabhan** (Member, IEEE) received the B.Tech. degree in electrical and electronics engineering and the M.Tech. degree in electrical engineering from the University of Calicut, Malappuram, Kerala, India, in 2007 and 2010, respectively, and the Ph.D. degree in electrical and computer engineering from the University of Waterloo, Waterloo, ON, Canada, in 2019.



He was a Lecturer and an Assistant Professor with the Department of Electrical and Electronics Engineering, Vidya Academy of Science and Technology, Thrissur, Kerala, from 2009 to 2014, and a Postdoctoral Fellow with the University of Waterloo from 2019 to 2021. He also served as an Advisor for Market Development with the Independent Electricity System Operator (IESO), Toronto, ON, Canada from October 2021 to December 2021. He is currently working as an Engineer/Scientist with EPRI International, Palo Alto, CA, USA. His research interests include demand response, energy storage applications, electricity market modeling and design, and optimization of power systems.

**Walter Violante** received the bachelor's and master's degrees in electrical engineering from the Politecnico di Bari, Bari, Italy, in 2016 and 2019, respectively.



He works in O&M of high voltage and HVdc plants at Terna, Rome, Italy, the Italian transmission system operator. His research interests include modeling, simulation, control, and optimization of power systems.